
ImDrug: A Benchmark for Deep Imbalanced Learning in AI-aided Drug Discovery

Lanqing Li^{1,2,†*} Liang Zeng^{1,3,†} Ziqi Gao^{1,4,†} Shen Yuan^{1,5,†} Yatao Bian¹
Bingzhe Wu¹ Hengtong Zhang¹ Yang Yu¹ Chan Lu¹ Wei Liu¹ Hongteng Xu⁵
Jia Li⁴ Peilin Zhao¹ Pheng-Ann Heng²

¹Tencent AI Lab, China

²The Chinese University of Hong Kong, China

³Tsinghua University, China

⁴Hong Kong University of Science and Technology, China

⁵Renmin University of China, China

September 19, 2022

Abstract

The last decade has witnessed a prosperous development of computational methods and dataset curation for AI-aided drug discovery (AIDD). However, real-world pharmaceutical datasets often exhibit highly imbalanced distribution, which is largely overlooked by the current literature but may severely compromise the fairness and generalization of machine learning applications. Motivated by this observation, we introduce ImDrug, a comprehensive benchmark with an open-source Python library which consists of 4 imbalance settings, 11 AI-ready datasets, 54 learning tasks and 16 baseline algorithms tailored for imbalanced learning. It provides an accessible and customizable testbed for problems and solutions spanning a broad spectrum of the drug discovery pipeline such as molecular modeling, drug-target interaction and retrosynthesis. We conduct extensive empirical studies with novel evaluation metrics, to demonstrate that the existing algorithms fall short of solving medicinal and pharmaceutical challenges in the data imbalance scenario. We believe that ImDrug opens up avenues for future research and development, on real-world challenges at the intersection of AIDD and deep imbalanced learning¹.

1 Introduction

On average, it costs over a decade and up to about 3 billion USD to bring a new drug to the market [1]. The current drug discovery pipeline devised by domain experts, which largely relies on labor-intensive wet-lab trials, delivers a commercialized drug at only approximately 10% success rate [2] despite substantial investment. AI-aided drug discovery (AIDD) as an emerging area of research, has the potential in revolutionizing the pharmaceutical industry by offering highly efficient and data-driven computational tools to identify new compounds and model complex biochemical mechanisms, thus considerably reducing the cost of drug discovery [3]. A key to the success of this dry-lab paradigm is

*Correspondence to: Lanqing Li <lanqingli1993@gmail.com>

[†]Equal contribution.

¹Source code and datasets are available at: <https://github.com/DrugLT/ImDrug>.

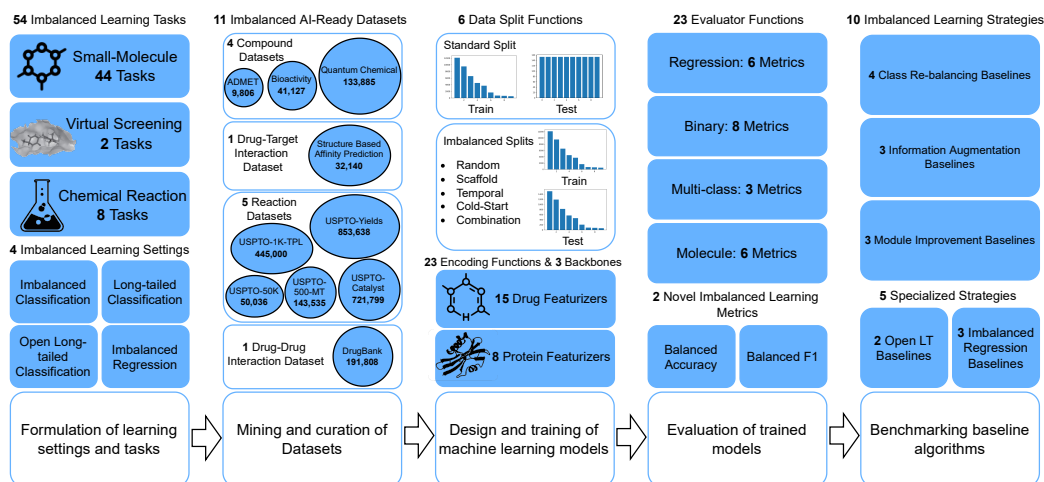


Figure 1: **Overview of the ImDrug pipeline.** ImDrug provides datasets, modules and utilities for training and evaluating imbalanced learning algorithms for AIDD in a plug-and-play manner. It supports research and development for solutions to real-world drug discovery problems such as molecular modeling, drug-target interaction and retrosynthesis.

deep learning. To date, AI driven by deep neural networks has significantly advanced the state-of-the-art in pharmaceutical applications ranging from de novo drug design [4, 5], ADMET prediction [6, 7], retrosynthesis [8–11], protein folding and design [12–14] to virtual screening [15–17].

Despite the success of deep learning in AIDD, by examining a myriad of medicinal chemistry databases and benchmarks [6, 10, 11, 18–21], we observe that these curated data repositories ubiquitously exhibit imbalanced distributions regardless of the specific tasks and domains². This observation is reminiscent of the power-law scaling in networks [22] and the Pareto principle [23], which poses significant challenges for developing unbiased and generalizable AI algorithms [24].

Deep imbalanced learning [25, 26], a paradigm aiming to address the aforementioned challenges, remains relatively understudied [27] despite its importance and practicality for real-world applications. In the scenario of extreme imbalance ratio and large number of classes, it is closely connected to long-tailed recognition [28, 29] and subpopulation shift [30, 31]. However, recent work mostly focuses on Computer Vision (CV) tasks with convolutional neural networks [32–36], where state-of-the-art performance has become relatively saturated [28, 37]. To call attention to the prevalent imbalance issue in the pharmaceutical domain and drive algorithmic innovation for real-world problems, we fill the gap by presenting a comprehensive benchmark for Deep **Imbalanced Learning** in AI-aided **Drug Discovery**, ImDrug for brevity.

Present work. With ImDrug, we provide a platform to systematically implement and evaluate deep imbalanced learning across a whole spectrum of therapeutics, covering 11 AI-ready datasets and 54 learning tasks (Fig. 1). Inspired by the recent progress and literature on long-tailed visual recognition [28], we benchmark 10 competitive baselines which can be divided into 3 categories: class re-balancing, information augmentation and module improvement. In addition to the imbalanced and long-tailed classification, ImDrug also incorporates 2 realistic but more challenging imbalanced settings, namely open long-tailed classification [33] and imbalanced regression [38]. These settings require intrinsically different treatments of data and label distribution, for which our benchmark sheds light on future innovation of effective algorithms.

The canonical data splitting of imbalanced learning termed the standard split in ImDrug (Fig. 1), is to randomly sample a training set while retaining a *balanced* test set to ensure equality of all classes [28, 39]. However, for highly imbalanced (long-tailed) datasets, such splitting severely restricts the size of the test set by forcing the sample number of majority classes to equal that of minority classes. To improve the quality of evaluation statistics, we introduce 5 imbalanced data split functions following the best practice in chemical sciences to cover more realistic out-of-distribution scenarios, which allows for significantly larger test sets. We argue that commonly reported metrics such as accuracy and AUROC can be over-optimistic under imbalanced distributions. Accordingly,

²For visualization of the imbalanced datasets, check Appendix for more details.

two imbalanced learning metrics, *balanced accuracy* [40, 41] and a novel measure *balanced F1*, are proposed to provide better insight of the evaluations due to their robustness to test distributions.

In summary, we make three key **contributions** in this work:

- *Systematic and focused study at the intersection of AIDD and deep imbalanced learning.* We identify data imbalance as a major challenge in AIDD. In response, we build ImDrug, to our best knowledge the first comprehensive platform for benchmarking up-to-date deep imbalanced learning methods across datasets and tasks spanning the drug discovery lifecycle. Our analysis shows that there is ample room for further algorithmic improvement.
- *Accessible framework for configuring customized datasets and algorithms.* We provide a Python package and unified configuration tools to allow for the curation of new datasets and imbalanced learning algorithms, with a scalable modular and hierarchical design.
- *Extended scope and novel metrics.* In addition to the conventional imbalanced and long-tailed classification, ImDrug encompasses 2 practically important and challenging settings with an empirical study of the corresponding specialized algorithms. It features up-to-date chemical reaction datasets with multi-class labels to enable benchmarks of long-tailed learning methods. Moreover, we identify the limitation of standard data splits and evaluate baselines on various imbalanced splits via two robust metrics, balanced accuracy and newly proposed balanced F1.

2 Related Work

ImDrug is the first systematic and unified platform targeting deep imbalanced learning in AIDD. To date, the researches on imbalanced learning and AIDD follow two separate lines with little overlap, which we briefly review in this section.

Relation to imbalanced learning literature and benchmarks. Imbalanced learning, or long-tailed learning in extreme cases (Table 1), remains a long-standing problem in machine learning [25, 26]. He and Garcia [25] partition the imbalanced learning methods into 5 categories, including sampling, cost-sensitive, kernel-based, active learning and other methods. Later, Krawczyk [26] distinguishes 3 general approaches to learning from imbalanced data: *data-level methods* by re-balancing samples, *algorithm-level methods* by algorithmic bias alleviation and adaptation to skewed distribution, and *hybrid methods* that combine the advantages of two previous groups. Most recently, by going through the bulk of deep long-tailed recognition methods published since 2016, Zhang et al. [28] make a new taxonomy consisting of class re-balancing, information augmentation and module improvement with 9 sub-classes. In this work, we implement and benchmark 10 competitive imbalanced learning methods to better reflect the up-to-date progress in this field.

Relation to AIDD repositories. For drug discovery, there exists a myriad of large-scale databases with different focuses. ChEMBL [19, 42] contains over 2.1 million compounds and 18.6 million bioassay records of their activities. BindingDB [43] provides a collection of binding affinity data between small molecules and proteins. USPTO [18] curates nearly 2 million reaction data mined from US patent applications. These biorepositories are naturally imbalanced and serve as valuable resources for ImDrug. However, they require careful pre-processing to be amenable to deep learning models, due to inconsistent data representations and noisy labels.

Based on the preceding raw databases, several AI-ready datasets and standard benchmarks have been built recently. MoleculeNet [6] provides among the first large-scale repositories for molecular machine learning and quantitative structure-activity relationship (QSAR) [44] modeling, with benchmarks for classical machine learning and graph-based models. The authors briefly discuss the class imbalance in the datasets and suggested using AUROC and AUPRC for evaluation. The settings were largely inherited in follow-up works such as TDC [20], which extends the scope of modalities and learning tasks to full coverage of therapeutics pipelines. Our work builds upon the tiered design and implementation of TDC and introduces extra datasets for virtual screening [21] and chemical reactions. It features a series of latest USPTO datasets [10, 11, 18, 20, 45] to support *multi-class prediction* of reaction type, template, catalyst and yield, in contrast to the *binary classification tasks* in MoleculeNet and TDC. Moreover, ImDrug carries out a systematic and focused study of deep imbalanced learning in AIDD with comprehensive settings and newly proposed metrics. We highlight the observations that data imbalance poses a key obstacle for developing trustworthy AIDD solutions, justifying the need and opportunity for algorithmic innovation at the intersection of AIDD and deep imbalanced learning.

3 Overview

3.1 High-level Design

The design principle of ImDrug is to provide a platform with full coverage of the algorithm development lifecycle in AIDD. From a high-level view, the five-stage ImDrug pipeline illustrated in Fig. 1 consists of a superposition of efforts in two orthogonal dimensions: *curation of AIDD datasets/learning tasks* and *benchmarking imbalanced learning algorithms*.

3.1.1 Tiered Design of Data & Learning Tasks

For organizing datasets and learning tasks, we employ a three-level hierarchical structure. At the top level, inspired by TDC [20], we categorize 54 learning tasks into three prediction problems:

- **Single-instance prediction:** Predictions based on individual biomedical entities, including 44 tasks on small molecules.
- **Multi-instance prediction:** Predictions based on multiple heterogeneous entities, including 2 tasks on virtual screening.
- **Hybrid prediction:** Predictions based on a set of homogeneous entities, which can be either aggregated (*e.g.*, string or graph concatenation) to perform single-instance prediction, or separately encoded to apply multi-instance prediction, including 7 tasks on chemical reactions and 1 on drug-drug interaction.

At the middle level, each prediction problem above is assigned with a collection of datasets:

- 4 compound datasets for prediction of the ADMET (absorption, distribution, metabolism, excretion and toxicity), bioactivity and quantum chemical properties.
- 1 drug-target interaction dataset for prediction of the protein-ligand binding affinity.
- 5 reaction datasets for prediction of the chemical reaction type, template, catalyst and yield. 1 dataset for drug-drug interaction prediction.

A detailed summary of the 11 datasets statistics is shown in Appendix. At the bottom level, we provide data processing utilities involving 6 split functions and 23 featurizers customized for drug and protein. Besides the standard splitting with balanced test set, ImDrug offers 5 imbalanced data split functions to account for settings such as out-of-distribution [21] and continual learning [46], with improved quality of evaluation statistics by enabling a significantly larger test set in the highly imbalanced scenario. Additionally, our proposed metrics in Sec. 3.2 ensure fairness with a mathematical guarantee that testing on imbalanced splits is equivalent to evaluation on a balanced test set (Thm. 3.1).

3.1.2 Imbalanced Learning Settings

For benchmarking imbalanced learning algorithms, to start with, we define the imbalanced learning problem as follows. Consider $\{x_i, y_i\}_{i=1}^n$ as an imbalanced dataset consisting of n sample-label pairs drawn from K classes with $n = \sum_{k=1}^K n_k$, where n_k denotes the number of data points of class k and $\pi_k = n_k/n$ represents the label frequency of class k . Without loss of generality, we assume the classes are sorted by cardinality in decreasing order [28], *i.e.*, if $i < j$, then $n_i \geq n_j$, and $n_1 \gg n_k$. We denote by n_1/n_K the imbalance ratio of the dataset.

Based on the setup above, we formulate 4 realistic and practically important imbalanced learning settings summarized in Table 1. Besides the regular imbalanced classification, which is usually measured by metrics like accuracy, F1 score, and AUROC, we observe that some AIDD datasets contain an extremely large number of classes with high imbalance ratio. For instance, in terms of reaction type classification, USPTO-50k [45], USPTO-500-MT [11] and USPTO-1k-TPL [10] have 10, 500 and 1000 classes with imbalance ratio 22.6, 285.0 and 117.4 respectively. These datasets exhibit power-law scaling of label frequency distributions, which are attributed to the long-tailed (LT) classification protocol of ImDrug. Conventionally, evaluations on LT classification report statistics for the head, middle, tail, and overall classes separately.

Additionally, open long-tailed classification (Open LT) [33] as the third setting, introduces more challenging problems by demanding the algorithms to not only strike the balance between majority and minority classes, but also be able to generalize to unseen (open) classes at test time. This

Table 1: Comparison between the 4 imbalanced learning settings investigated in ImDrug.

Setting	Label Type	Imbalance Ratio	# Classes	Evaluation Metrics	Open Class at Test Time
Imbalanced Classification	Categorical	Low	< 10	Acc, F1, AUROC	✗
Long-Tailed Classification	Categorical	High	≥ 10	Acc, F1, AUROC (+head, middle, tail)	✗
Open Long-Tailed Classification	Categorical	High	≥ 10	Acc, F1, AUROC (+head, middle, tail, open)	✓
Imbalanced Regression	Continuous	N/A	N/A	MSE, MAE (+head, middle, tail)	N/A

scenario is closely connected to the out-of-distribution studies of AIDD [21] and cost-sensitive online classification [47]. Besides the shift of class labels implemented in ImDrug, examples of open-set distribution shifts in drug discovery include domain shift of molecular size and scaffold, cold-start of new protein targets, and temporal shift of reported reaction patents as in Fig. 1.

The last setting, imbalanced regression, calls for attention of the data imbalance issue in continuous label space [38]. As opposed to the categorical target space of classification tasks, the continuous label spectrum inherently enforces a meaningful distance between targets, which has implications for how one should interpret data imbalance. This setup is not as well explored but extends the scope of ImDrug to a new set of real-world AIDD applications, such as the prediction of quantum chemical properties [48, 49], protein-ligand binding affinity [21] and reaction yields [11].

3.2 Evaluation Metrics

For conventional imbalanced classification and regression in domains like Computer Vision, by treating all classes equally, a balanced test set is selected [28, 38]. However, in highly imbalanced dataset (*i.e.*, high imbalance ratio), such criterion severely constrains the size of the test set. Given the Central Limit Theorem and the fact that the uncertainty of the point-estimated mean scales with $1/\sqrt{n}$ (n being the number of samples), ideally we would like to have a much larger test set, *e.g.*, 10-20% of the whole dataset to achieve satisfactory statistical significance at evaluation.

However, employing traditional metrics like accuracy and F1 score on an imbalanced test set can be problematic in two ways [41]: first, it does not allow for the derivation of meaningful confidence intervals; second, it leads to an optimistic estimate in presence of a biased classifier. To address the dilemma, we adopt the balanced accuracy [40, 41] and propose a novel balanced F1 score which can be used as unbiased measure on any imbalanced test sets. To formalize our proposed metric, we define the balanced multi-class precision analogous to the calibrated precision introduced in [50]:

Definition 1. Given a test set $\{x_i, y_i\}_{i=1}^n$ of n samples drawn from K classes and the corresponding predicted labels $\{\hat{y}_i\}_{i=1}^n$, the balanced accuracy/recall and precision for class k are defined as:

$$\text{Balanced-Acc/Rec} := \frac{1}{K} \sum_{k=1}^K \text{Rec}_k = \frac{1}{K} \sum_{k=1}^K \frac{\sum_{i=1}^n \mathbb{1}(y_i = k, \hat{y}_i = k)}{\sum_{i=1}^n \mathbb{1}(y_i = k)} \quad (1)$$

$$\text{Balanced prec for class } k := \frac{\sum_{i=1}^n \mathbb{1}(y_i = k, \hat{y}_i = k)}{\sum_{i=1}^n \mathbb{1}(y_i = k, \hat{y}_i = k) + \sum_{j \neq k} \sum_{i=1}^n \pi_{jk} \mathbb{1}(y_i = j, \hat{y}_i = k)}, \quad (2)$$

where Rec_k stands for the recall for class k and the calibration factor $\pi_{jk} = \sum_{i=1}^n \mathbb{1}(y_i = k) / \sum_{i=1}^n \mathbb{1}(y_i = j) = n_k / n_j$ is the ratio between the label frequencies of class k and j . When $\pi_{jk} \equiv 1$, *i.e.*, the dataset is perfectly balanced, Eqn. 2 recovers the conventional one-vs-all precision for class k .

Note that, unlike the balanced precision, the balanced recall for class k is equivalent to the conventional one-vs-all recall for the same class, since its calculation does not involve the support of other classes, which induces the following theorem:

Theorem 3.1. Let Rec_k and Prec_k denote the recall and balanced precision for class k . Given a trained predictor, the evaluated balanced F1 score

$$\text{Balanced-F1} := \frac{1}{K} \sum_{k=1}^K \frac{2 \times \text{Rec}_k \times \text{Prec}_k}{\text{Rec}_k + \text{Prec}_k} \quad (3)$$

is invariant to label distribution shift on any test set, where samples of each class are drawn *i.i.d* from a fixed distribution.

Proof. See Appendix B. □

3.3 Imbalanced Learning Baselines

In this section, we provide a brief review of benchmarked baseline methods for the 4 imbalanced learning protocols summarized in Table 1. A comprehensive description can be found in Appendix.

3.3.1 Baselines of Imbalanced & Long-Tailed Classification

Besides the vanilla baseline trained by the softmax cross-entropy loss, following the taxonomy proposed by Zhang et al. [28], we consider 10 baselines in 3 families of conventional deep imbalanced/long-tailed classification methods: 4 for class re-balancing (**Cost-Sensitive Loss (CS)** [51], **Class-Balanced Loss (CB_F)** [34], **Balanced Softmax (BS)** [52], **Influence-Balanced Loss (IB)** [53]), 3 for information augmentation (**Mixp** [54], **Remix** [55], **DiVE** [56]) and 3 for module improvement (**CDT** [57], **Decoupling** [58], **BBN** [59]). For implementation, we employ a modular design based on [29] and choose the baselines which can be realized as individual “trick” in terms of loss functions (re-weighting), data samplers (re-sampling, two-stage training) or instance combiners (mixup training). The selection of baselines reflects a notable scientific progress and paradigm shift of imbalanced learning algorithms from 2002 to date.

3.3.2 Baselines of Open LT & Imbalanced Regression

Open LT can be regarded as a variant of conventional long-tailed classification with unseen and out-of-distribution (OOD) tail classes in the test set. In principle, all aforementioned baselines for imbalanced classification can be seamlessly transferred to this setting. However, the extra challenge posed by the protocol requires targeted remedies to OOD generalization to achieve state-of-the-art performance. Hence ImDrug includes 2 additional baselines for Open LT: **OLTR** [33] and **IEM** [60].

Imbalanced Regression can be reduced to conventional imbalanced classification by naively dividing the continuous label space into multiple consecutive bins as classes. In this way, many baselines in Sec. 3.3.1 can be adapted by replacing the classification head with a regression head. However, such trivial transformation undermines the intrinsic topology of labels induced by the Euclidean distance, leading to sub-optimal performance [38]. In ImDrug, we experiment with 3 extra baselines specialized at solving this particular challenge: **Focal-R** [38], **LDS** [38] and **FDS** [38].

4 Experiments

In experiments, we benchmark 11 baselines for conventional imbalanced & long-tailed classification (Sec. 3.3.1), as well as 5 additional baselines tailored for open LT and imbalanced regression, by reporting the 2 proposed balanced accuracy and balanced F1 measures along with the conventional AUROC. All average performance with standard deviations is evaluated over 3 random seeds. For featurization, we choose GCN [61] as the default backbone and implement the input graph encoding via the DGL library [62]. In ImDrug, due to the multi-modal nature of molecular data, we experiment with MLP, Transformer, and GCN [61] for numeric (*e.g.*, Morgan Fingerprint [63]), sequence (*e.g.*, SMILES [64]) and graph feature representations respectively. Due to space limitations, additional empirical studies such as ablations of the backbone models are provided in Appendix.

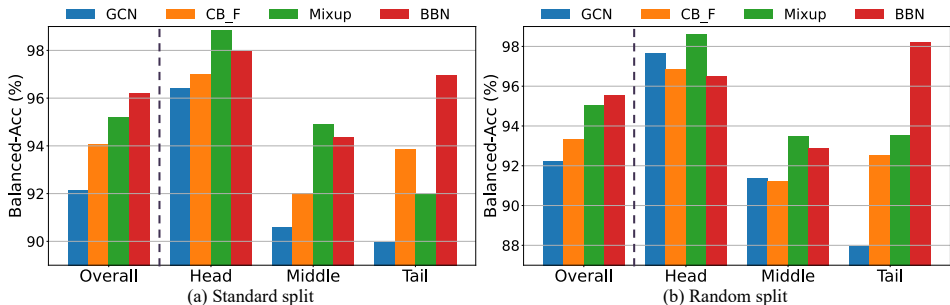


Figure 2: Performance of single-instance prediction for the dataset USPTO-50K of overall, head, middle and tail under standard and random splits. Balanced accuracy for 4 baseline methods on different class subsets are shown.

Table 2: **Results for random and standard splits on 4 ImDrug classification datasets.** We perform binary classification on HIV (single-instance prediction) and SBAP (multi-instance prediction), and long-tailed classification on USPTO-50K (single-instance prediction) and DrugBank (multi-instance prediction). For each split and metric, the best method is **bolded** and the second best is underlined. Four classical machine learning baselines with ECFP4 [63] input features are added, all of which under-perform the neural network-based methods.

		HIV[6]				SBAP[21]				USPTO-50K[45]				DrugBank[65]			
		Balanced-Acc	Balanced-F1	AUROC	Balanced-Acc	Balanced-F1	AUROC	Balanced-Acc	Balanced-F1	AUROC	Balanced-Acc	Balanced-F1	AUROC	Balanced-Acc	Balanced-F1	AUROC	
# Graphs		41,127				32,140				50,036				191,808			
# Average nodes		25.51				32.60				25.03				26.43			
# Average edges		54.94				103.94				78.29				83.21			
# Classes		2				2				10				86			
Imbalance ratio		27.50				36.77				65.78				216.96			
Metric		Balanced-Acc	Balanced-F1	AUROC	Balanced-Acc	Balanced-F1	AUROC	Balanced-Acc	Balanced-F1	AUROC	Balanced-Acc	Balanced-F1	AUROC	Balanced-Acc	Balanced-F1	AUROC	
Random	Vanilla GCN	71.89	69.82	83.03	77.50	76.39	95.07	92.23	92.20	99.76	87.54	87.60	99.78				
	Random Forest	63.84	58.52	82.84	63.33	57.98	92.49	70.10	70.43	98.33	60.94	63.65	98.77				
	Decision Tree	57.98	49.13	64.52	51.72	37.12	73.60	65.98	66.49	81.40	56.25	59.41	78.14				
	SMOTE [66]	66.68	62.67	83.67	76.68	76.88	82.04	77.51	78.06	98.28	-	-	-				
	k-NN	62.95	57.20	72.43	74.94	73.59	75.11	64.26	65.02	92.63	48.51	51.43	88.87				
	Class-rebalancing	77.13	76.71	83.91	83.21	83.06	91.01	93.69	93.71	93.71	99.76	94.98	94.77	99.60			
	CB_F	73.14	72.66	82.23	81.02	79.88	94.59	93.32	93.33	99.49	93.71	93.79	99.31				
	CS	<u>77.04</u>	<u>76.66</u>	79.90	91.49	91.48	96.67	93.01	93.04	99.71	93.67	93.70	99.39				
	Mixup	73.06	70.62	82.99	78.38	77.41	95.81	95.03	95.04	99.77	92.15	91.78	99.84				
	Remix	74.43	72.19	81.09	79.58	78.49	95.01	94.83	94.84	95.26	94.47	94.32	99.76				
	DIVE	75.07	74.24	81.12	84.58	84.65	95.43	93.90	93.91	99.60	90.26	91.08	99.42				
	Module Improvement	71.67	69.52	82.95	78.92	78.17	95.58	93.92	93.92	93.92	99.78	94.54	94.32	99.52			
Decoupling	74.64	73.33	83.66	85.04	84.82	95.66	92.81	92.81	94.43	90.00	90.27	99.79					
IB	73.80	71.32	79.88	83.70	83.61	90.65	93.00	93.00	99.66	90.10	90.38	99.39					
BBN	76.50	76.36	81.65	<u>90.67</u>	<u>90.67</u>	<u>96.16</u>	95.57	95.56	99.67	92.55	92.54	99.48					
Vanilla GCN	71.24	68.99	80.99	77.29	76.21	94.70	92.15	92.15	92.15	99.54	89.38	86.96	98.09				
Random Forest	64.58	59.50	82.35	59.19	51.54	91.64	71.63	71.63	71.75	98.01	61.90	56.75	97.34				
Decision Tree	57.20	48.01	67.36	50.27	33.93	80.08	72.33	72.33	72.16	84.63	52.38	44.96	76.37				
SMOTE [66]	67.23	63.40	82.91	70.27	68.65	92.62	79.07	79.07	79.56	98.33	-	-	-				
k-NN	64.02	58.79	78.78	62.43	56.66	78.99	67.91	68.56	68.56	92.79	42.86	38.02	88.66				
Class-rebalancing	75.04	74.85	79.60	88.41	88.38	95.16	93.62	93.62	93.59	99.63	94.69	92.58	98.93				
CB_F	71.57	69.57	80.59	84.70	83.78	94.93	94.07	94.11	94.27	99.27	90.55	88.09	97.77				
CS	76.95	76.39	81.06	89.79	89.78	95.61	92.73	92.73	92.76	99.62	<u>94.69</u>	<u>92.89</u>	98.50				
Information augmentation	71.48	69.31	81.18	79.69	78.04	94.99	95.21	95.19	95.19	99.65	85.45	83.48	99.13				
Mixup	71.59	69.47	81.53	77.90	76.71	94.56	<u>95.27</u>	<u>95.25</u>	<u>95.25</u>	99.57	89.93	87.46	98.78				
Remix	74.16	72.69	81.06	86.69	86.65	93.41	94.03	94.00	94.00	99.43	89.95	87.46	98.33				
DIVE	71.87	68.94	80.47	81.51	80.98	94.14	93.79	93.78	93.78	99.65	91.15	88.29	98.80				
Module Improvement	73.14	71.52	80.00	69.58	66.33	90.99	92.64	92.60	92.60	99.56	89.97	87.30	98.61				
Decoupling	75.34	75.14	80.16	84.87	84.87	91.41	91.51	91.55	91.55	98.90	89.98	87.14	98.39				
IB	73.50	73.39	80.96	<u>88.49</u>	<u>88.45</u>	<u>94.02</u>	96.23	96.25	96.25	99.75	95.28	93.61	98.52				
BBN	73.50	73.39	80.96	88.49	88.45	94.02	96.23	96.25	96.25	99.75	95.28	93.61	98.52				

4.1 Results on Imbalanced & Long-Tailed Classification

Table 2 reports the average performance of imbalanced learning baselines on 2 binary (*aka.*, imbalanced) classification and 2 multi-class (*aka.*, long-tailed) classification datasets. For the 2 proposed balanced metrics, we observe a high correlation between the performance on balanced standard split and imbalanced random split (Fig. 3 for apple-to-apple comparison), which is in agreement with

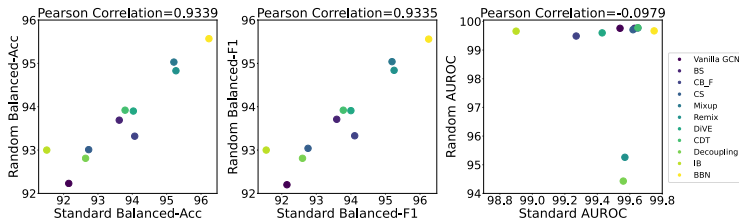


Figure 3: **Comparison of the baseline performance for standard and random splits on USPTO-50K under single-instance prediction**, in terms of balanced accuracy, balanced F1 and AUROC. The 2 proposed balanced metrics exhibit a good Pearson’s R correlation between the two splits (0.9339, 0.9335), which is significantly higher than AUROC (0.0979).

the theory (Thm. 3.1) that both metrics are insensitive to label distributions. Moreover, almost all baseline methods outperform the vanilla GCN baseline, demonstrating the effectiveness of deep imbalanced learning. However, we observe that the SOTA models do not work well consistently across the ImDrug data collections. For example, the information augmentation algorithms are most effective on USPTO-50K but subpar on the others. Whereas the class-rebalancing approaches are highly competitive on HIV and DrugBank. Module improvement methods such as BBN exhibit the most consistent and superior performance overall, which aligns with the empirical findings by Zhang et al. [28] in the CV domain and explains the paradigm shift of deep imbalanced learning towards this direction in recent years [28].

Besides the results on all classes, Fig. 2 breaks down the performance of 4 baselines on USPTO-50K into the head, middle, and tail classes. Evidently, effective imbalanced learning methods like BBN and Remix increase the overall performance by consistently improving on all class subsets, with the most significant gain on the tail classes.

By comparing the results on the three evaluation metrics, we observe consistent rankings, especially between the two balanced metrics (also shown in Fig. 5). Moreover, on these highly-imbalanced AIDD datasets, AUROC offers over-optimistic results and is typically insensitive to different baselines. In contrast, *the proposed balanced metrics more effectively highlight the challenges posed by the imbalanced settings*, by significantly up-weighting the contribution from the minority classes and hard samples. The fact that even the SOTA algorithms fail to reach 80% accuracy for binary classification on HIV, indicates there is ample room for methodological innovation and improvement for real-world AIDD problems.

Table 3: **Results on Open LT under standard split.** The proportions of open classes in USPTO-50K (single-instance prediction) and DrugBank (multi-instance prediction) are both 0.2.

	USPTO-50K			DrugBank		
	Balanced-Acc	Balanced-F1	AUROC	Balanced-Acc	Balanced-F1	AUROC
Vanilla GCN	85.82±0.42	81.38±0.41	94.18±0.066	91.72±0.28	91.75±0.33	99.07±0.015
BS	85.88±1.02	81.44±0.90	94.22±0.68	94.71±0.044	94.14±0.05	99.11±0.03
CB_F	86.77±0.99	82.2±1.22	94.16±0.08	93.17±0.43	92.84±0.40	98.80±0.11
Remix	87.92±0.23	83.40±0.21	93.91±0.13	92.68±0.83	92.75±0.59	99.59±0.40
IB	86.06±1.14	81.63±1.09	94.15±0.040	92.95±0.31	92.31±0.31	99.03±0.04
BBN	87.86±0.14	83.32±0.13	94.07±0.19	94.52±0.33	93.96±0.34	98.92±0.07
OLTR	89.21±0.75	85.11±0.38	96.69±0.12	95.37±0.30	94.92±0.16	99.79±0.09
IEM	89.99±0.29	85.46±0.20	96.74±0.09	95.77±0.16	95.16±0.15	99.64±0.08
OLTR+BBN	91.18±0.11	87.97±0.60	97.72±0.56	96.84±1.59	96.12±0.93	99.89±0.69
IEM+BBN	90.66±0.41	86.03±0.75	96.64±1.03	96.06±0.76	95.59±0.96	99.77±0.12

4.2 Results on Open LT & Imbalanced Regression

For Open LT setting, we further conduct experiments on 2 multi-class classification datasets, and report the mean with standard deviation under random split in Table 3. Observations are summarized in two aspects. First, deep imbalanced learning methods consistently outperform the vanilla GCN baseline in this setting, which demonstrates their effectiveness. Second, specifically designed algorithms for Open LT, such as OLTR, outperform methods for conventional imbalanced learning. Moreover, the fact that OLTR and IEM can directly operate on the processed embeddings of conventional baselines like BBN makes the combination of these tricks synergistic, which aligns with the observations in [28, 29]. Indeed, OLTR+BBN outperforms the BBN baseline by up to 2.82% on average, which highlights the benefit for exploring the combinatorial design space of baselines across various imbalanced learning settings.

For imbalanced regression, we report the mean results with standard deviations in terms of MSE and MAE on 2 imbalanced regression datasets in Table 4. We find that algorithms tailored for imbalanced regression outperform all conventional imbalanced classification methods. In particular, FDS stands out by beating all other competing methods in this experimental setting. However, despite the effectiveness of FDS, the improvements are still marginal on datasets like QM9, which calls for more effective solutions targeting imbalanced regression.

4.3 Evaluations of the Specific Designs

Besides the general findings on the 4 imbalanced learning settings, in this section, we assess the effectiveness of the specific utilities introduced by ImDrug. With experiments and analysis, we aim to address the following two core questions:

- **Q1:** Can ImDrug provide meaningful proxies of the real-world challenges in AIDD? (Sec. 4.3.1)
- **Q2:** Can ImDrug address the loss of efficacy of conventional metrics (*e.g.*, regular accuracy) on imbalanced test sets? (Sec. 4.3.2)

4.3.1 Observations on the OOD Splits

One of the most pressing real-world challenges in AIDD is OOD shifts [20, 21], which is prevalent in QSAR problems such as small-to-large molecule generalization for ADMET prediction, cold-start of protein targets (*e.g.*, unseen antigens of COVID-19) for drug-target interaction and predictions of unknown reaction types for retrosynthesis. Fortunately, as in Fig. 1, ImDrug provides testbeds for these domain-specific challenges with 5 extra data split functions.

Among them, the scaffold split poses harder challenges than random split for single-instance predictions by assigning the compounds with an identical backbone (Murcko scaffold [67]) to the same train/valid/test sets, making the splitted datasets more structurally different. For USPTO repositories curated from chemical reactions with patent date information, temporal split mimics real-world drug discovery challenges by assigning all samples published before a specific point in time to the training

Table 4: **Results on imbalanced regression under standard split.** We report the average performance on SBAP-Reg (multi-instance prediction) and QM9 (single-instance prediction) in terms of mean MSE and MAE with standard deviation in this setting.

	SBAP-Reg		QM9	
	MSE	MAE	MSE	MAE
Vanilla GCN	1.66 \pm 1.03	0.92 \pm 0.25	76.17 \pm 42.82	6.57 \pm 1.92
Mixup	1.10 \pm 0.51	0.78 \pm 0.17	82.35 \pm 36.86	6.59 \pm 1.46
BBN	1.52 \pm 1.57	0.89 \pm 0.38	59.42 \pm 14.39	6.02 \pm 0.77
Focal-R	1.38 \pm 1.08	0.84 \pm 0.31	94.29 \pm 57.38	7.23 \pm 2.65
LDS	1.36 \pm 1.16	0.78 \pm 0.26	16.01\pm6.58	2.73\pm0.03
FDS	0.59\pm0.09	0.54\pm0.02	60.81 \pm 33.52	5.63 \pm 1.53

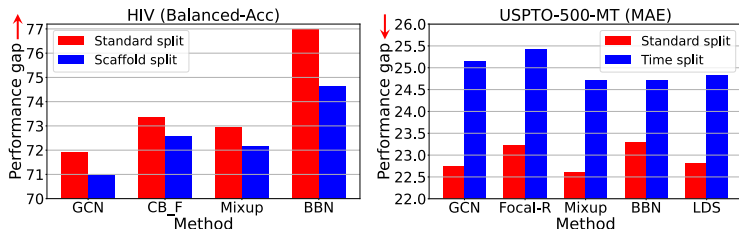


Figure 4: **Evaluations of baselines for binary classification** on HIV with scaffold split (**left**), and imbalanced regression on USPTO-500-MT with temporal split (**right**). Compared to the in-distribution standard split, the OOD splits on average induce performance gaps of 1.22% \downarrow in balanced accuracy and 2.03% \uparrow in MAE, respectively.

set and those published later to the test set, thus enforcing OOD in the temporal dimension. We investigated these two OOD splits on HIV and USPTO-500-MT respectively. As shown in Fig. 4, both splits result in consistently degraded performance across all baselines, highlighting the need for more advanced AIDD solutions addressing OOD and label imbalance simultaneously.

4.3.2 Observations on the Proposed Metrics

As measures of model discriminative power, accuracy and AUROC are the two most commonly used metrics for binary classification [20, 21, 28]. However, as shown in Table 2, they can be over-optimistic and insensitive to different models on highly imbalanced datasets. To overcome this challenge, Im-

Drug proposes to use balanced accuracy and balanced F1 score instead. To back up this design choice, we use reported AUROC on the *balanced test set* of standard split as the gold standard or anchor points, and plot the corresponding values of accuracy as well as balanced accuracy on the *imbalanced test set* of random split for comparison. Illustrated in Fig. 5, AUROC on standard split achieves good agreement with *balanced accuracy* on random split (Pearson’s $R = 0.4364$), whereas the correlation between that and *regular accuracy* is significantly lower (Pearson’s $R = 0.2092$). Moreover, the two proposed balanced metrics on random split reach excellent agreement (Pearson’s $R = 0.9999$), demonstrating the effectiveness of our novel balanced F1 score on imbalanced distributions as well.

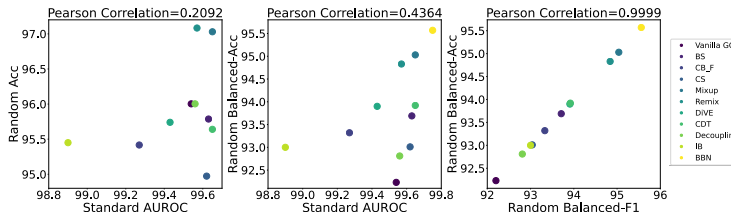


Figure 5: **Pearson’s correlations** between the proposed metrics and the commonly used ones on USPTO-50K. Points in figure are plotted for 11 baselines in Table 2.

5 Conclusion

In this work, motivated by the observed prevalence of imbalanced distribution of the real-world pharmaceutical datasets, we present ImDrug, a comprehensive platform for systematic model development and benchmarking to facilitate future research in AIDD. Unfortunately, targeted at the intersection of AIDD and deep imbalanced learning, we find that this subject has not received sufficient attention by the vast majority of work on ML modeling in either field alone. Through extensive experiments, it is shown that the existing algorithms as well as evaluation metrics leave sufficient room for improvement to be truly applicable in practice. We hope that this paper offers valuable insight for the machine learning and AIDD community as a whole, to think more critically about the importance and challenges of building trustworthy solutions to real-world AIDD problems. Continued development of ImDrug such as incorporating 3D-structured features, pre-trained model baselines, novel metrics for imbalanced regression and benchmarks for generation tasks will be supported to enrich this interdisciplinary and promising area of research.

References

- [1] Sudeep Pushpakom, Francesco Iorio, Patrick A Eyers, K Jane Escott, Shirley Hopper, Andrew Wells, Andrew Doig, Tim Williams, Joanna Latimer, Christine McNamee, et al. Drug repurposing: progress, challenges and recommendations. *Nature reviews Drug discovery*, 18(1):41–58, 2019.
- [2] Nihad AM Tamimi and Peter Ellis. Drug development: from concept to marketing! *Nephron Clinical Practice*, 113(3):c125–c131, 2009.
- [3] Petra Schneider, W Patrick Walters, Alleyn T Plowright, Norman Sieroka, Jennifer Listgarten, Robert A Goodnow, Jasmin Fisher, Johanna M Jansen, José S Duca, Thomas S Rush, et al. Rethinking drug design in the artificial intelligence era. *Nature Reviews Drug Discovery*, 19(5): 353–364, 2020.
- [4] Mariya Popova, Olexandr Isayev, and Alexander Tropsha. Deep reinforcement learning for de novo drug design. *Science advances*, 4(7):eaap7885, 2018.

- [5] Martin Simonovsky and Nikos Komodakis. Graphvae: Towards generation of small graphs using variational autoencoders. In Vera Kurková, Yannis Manolopoulos, Barbara Hammer, Lazaros S. Iliadis, and Ilias Maglogiannis, editors, *Artificial Neural Networks and Machine Learning - ICANN 2018 - 27th International Conference on Artificial Neural Networks, Rhodes, Greece, October 4-7, 2018, Proceedings, Part I*, volume 11139 of *Lecture Notes in Computer Science*, pages 412–422. Springer, 2018. doi: 10.1007/978-3-030-01418-6_41. URL https://doi.org/10.1007/978-3-030-01418-6_41.
- [6] Zhenqin Wu, Bharath Ramsundar, Evan N Feinberg, Joseph Gomes, Caleb Geniesse, Aneesh S Pappu, Karl Leswing, and Vijay Pande. Moleculenet: a benchmark for molecular machine learning. *Chemical science*, 9(2):513–530, 2018.
- [7] Yu Rong, Yatao Bian, Tingyang Xu, Weiyang Xie, Ying Wei, Wenbing Huang, and Junzhou Huang. Self-supervised graph transformer on large-scale molecular data. In Hugo Larochelle, Marc’Aurelio Ranzato, Raia Hadsell, Maria-Florina Balcan, and Hsuan-Tien Lin, editors, *Advances in Neural Information Processing Systems 2020, NeurIPS 2020, December 6-12, 2020, virtual*, 2020. URL <https://proceedings.neurips.cc/paper/2020/hash/94aef38441efa3380a3bed3faf1f9d5d-Abstract.html>.
- [8] Marwin H. S. Segler, Mike Preuss, and Mark P. Waller. Planning chemical syntheses with deep neural networks and symbolic AI. *Nat.*, 555(7698):604–610, 2018. doi: 10.1038/nature25978. URL <https://doi.org/10.1038/nature25978>.
- [9] Connor W Coley, William H Green, and Klavs F Jensen. Machine learning in computer-aided synthesis planning. *Accounts of chemical research*, 51(5):1281–1289, 2018.
- [10] Philippe Schwaller, Daniel Probst, Alain C Vaucher, Vishnu H Nair, David Kreutter, Teodoro Laino, and Jean-Louis Reymond. Mapping the space of chemical reactions using attention-based neural networks. *Nature machine intelligence*, 3(2):144–152, 2021.
- [11] Jieyu Lu and Yingkai Zhang. Unified deep learning model for multitask reaction predictions with explanation. *Journal of Chemical Information and Modeling*, 62(6):1376–1387, 2022.
- [12] John Jumper, Richard Evans, Alexander Pritzel, Tim Green, Michael Figurnov, Olaf Ronneberger, Kathryn Tunyasuvunakool, Russ Bates, Augustin Žídek, Anna Potapenko, et al. Highly accurate protein structure prediction with alphafold. *Nature*, 596(7873):583–589, 2021.
- [13] Minkyung Baek, Frank DiMaio, Ivan Anishchenko, Justas Dauparas, Sergey Ovchinnikov, Gyu Rie Lee, Jue Wang, Qian Cong, Lisa N Kinch, R Dustin Schaeffer, et al. Accurate prediction of protein structures and interactions using a three-track neural network. *Science*, 373(6557):871–876, 2021.
- [14] Drew H Bryant, Ali Bashir, Sam Sinai, Nina K Jain, Pierce J Ogden, Patrick F Riley, George M Church, Lucy J Colwell, and Eric D Kelsic. Deep diversification of an aav capsid protein by machine learning. *Nature Biotechnology*, 39(6):691–696, 2021.
- [15] Peng-Wei Hu, Keith CC Chan, and Zhu-Hong You. Large-scale prediction of drug-target interactions from deep representations. In *2016 international joint conference on neural networks (IJCNN)*, pages 1236–1243. IEEE, 2016.
- [16] Mostafa Karimi, Di Wu, Zhangyang Wang, and Yang Shen. Deepaffinity: interpretable deep learning of compound–protein affinity through unified recurrent and convolutional neural networks. *Bioinformatics*, 35(18):3329–3338, 2019.
- [17] Jaechang Lim, Seongok Ryu, Kyubyong Park, Yo Joong Choe, Jiyeon Ham, and Woo Youn Kim. Predicting drug–target interaction using a novel graph neural network with 3d structure-embedded graph representation. *Journal of chemical information and modeling*, 59(9):3981–3988, 2019.
- [18] Daniel Mark Lowe. *Extraction of chemical structures and reactions from the literature*. PhD thesis, University of Cambridge, 2012.

- [19] David Mendez, Anna Gaulton, A Patrícia Bento, Jon Chambers, Marleen De Veij, Eloy Félix, María Paula Magariños, Juan F Mosquera, Prudence Mutowo, Michał Nowotka, et al. ChEMBL: towards direct deposition of bioassay data. *Nucleic acids research*, 47(D1):D930–D940, 2019.
- [20] Kexin Huang, Tianfan Fu, Wenhao Gao, Yue Zhao, Yusuf Roohani, Jure Leskovec, Connor W. Coley, Cao Xiao, Jimeng Sun, and Marinka Zitnik. Therapeutics data commons: Machine learning datasets and tasks for drug discovery and development. In Joaquin Vanschoren and Sai-Kit Yeung, editors, *Proceedings of the Neural Information Processing Systems Track on Datasets and Benchmarks 1, NeurIPS Datasets and Benchmarks 2021, December 2021, virtual*, 2021. URL <https://datasets-benchmarks-proceedings.neurips.cc/paper/2021/hash/4c56ff4ce4aaf9573aa5dff913df997a-Abstract-round1.html>.
- [21] Yuanfeng Ji, Lu Zhang, Jiayang Wu, Bingzhe Wu, Long-Kai Huang, Tingyang Xu, Yu Rong, Lanqing Li, Jie Ren, Ding Xue, Houtim Lai, Shaoyong Xu, Jing Feng, Wei Liu, Ping Luo, Shuigeng Zhou, Junzhou Huang, Peilin Zhao, and Yatao Bian. DrugOOD: Out-of-Distribution (OOD) Dataset Curator and Benchmark for AI-aided Drug Discovery – A Focus on Affinity Prediction Problems with Noise Annotations. *arXiv e-prints*, art. arXiv:2201.09637, January 2022.
- [22] Albert-László Barabási and Réka Albert. Emergence of scaling in random networks. *science*, 286(5439):509–512, 1999.
- [23] Robert Sanders. The pareto principle: its use and abuse. *Journal of Services Marketing*, 1(2): 37–40, 1987.
- [24] Bo Li, Peng Qi, Bo Liu, Shuai Di, Jingen Liu, Jiquan Pei, Jinfeng Yi, and Bowen Zhou. Trustworthy AI: from principles to practices. *CoRR*, abs/2110.01167, 2021. URL <https://arxiv.org/abs/2110.01167>.
- [25] Haibo He and Edwardo A Garcia. Learning from imbalanced data. *IEEE Transactions on knowledge and data engineering*, 21(9):1263–1284, 2009.
- [26] Bartosz Krawczyk. Learning from imbalanced data: open challenges and future directions. *Progress in Artificial Intelligence*, 5(4):221–232, 2016.
- [27] Justin M Johnson and Taghi M Khoshgoftaar. Survey on deep learning with class imbalance. *Journal of Big Data*, 6(1):1–54, 2019.
- [28] Yifan Zhang, Bingyi Kang, Bryan Hooi, Shuicheng Yan, and Jiashi Feng. Deep long-tailed learning: A survey. *CoRR*, abs/2110.04596, 2021. URL <https://arxiv.org/abs/2110.04596>.
- [29] Yongshun Zhang, Xiu-Shen Wei, Boyan Zhou, and Jianxin Wu. Bag of tricks for long-tailed visual recognition with deep convolutional neural networks. In *Proceedings of the AAAI Conference on Artificial Intelligence*, volume 35, pages 3447–3455, 2021.
- [30] Steffen Bickel, Michael Brückner, and Tobias Scheffer. Discriminative learning for differing training and test distributions. In *Proceedings of the 24th international conference on Machine learning*, pages 81–88, 2007.
- [31] Solon Barocas and Andrew D Selbst. Big data’s disparate impact. *Calif. L. Rev.*, 104:671, 2016.
- [32] Chen Huang, Yining Li, Chen Change Loy, and Xiaoou Tang. Deep imbalanced learning for face recognition and attribute prediction. *IEEE transactions on pattern analysis and machine intelligence*, 42(11):2781–2794, 2019.
- [33] Ziwei Liu, Zhongqi Miao, Xiaohang Zhan, Jiayun Wang, Boqing Gong, and Stella X. Yu. Large-scale long-tailed recognition in an open world. In *IEEE Conference on Computer Vision and Pattern Recognition, CVPR 2019, Long Beach, CA, USA, June 16-20, 2019*, pages 2537–2546. Computer Vision Foundation / IEEE, 2019. doi: 10.1109/CVPR.2019.00264. URL http://openaccess.thecvf.com/content_CVPR_2019/html/Liu_Large-Scale_Long-Tailed_Recognition_in_an_Open_World_CVPR_2019_paper.html.

- [34] Yin Cui, Menglin Jia, Tsung-Yi Lin, Yang Song, and Serge Belongie. Class-balanced loss based on effective number of samples. In *Proceedings of the IEEE/CVF conference on computer vision and pattern recognition*, pages 9268–9277, 2019.
- [35] Muhammad Abdullah Jamal, Matthew Brown, Ming-Hsuan Yang, Liqiang Wang, and Boqing Gong. Rethinking class-balanced methods for long-tailed visual recognition from a domain adaptation perspective. In *Proceedings of the IEEE/CVF Conference on Computer Vision and Pattern Recognition*, pages 7610–7619, 2020.
- [36] Songyang Zhang, Zeming Li, Shipeng Yan, Xuming He, and Jian Sun. Distribution alignment: A unified framework for long-tail visual recognition. In *Proceedings of the IEEE/CVF Conference on Computer Vision and Pattern Recognition*, pages 2361–2370, 2021.
- [37] Yifan Zhang, Bryan Hooi, Lanqing Hong, and Jiashi Feng. Test-agnostic long-tailed recognition by test-time aggregating diverse experts with self-supervision. *arXiv preprint arXiv:2107.09249*, 2021.
- [38] Yuzhe Yang, Kaiwen Zha, Yingcong Chen, Hao Wang, and Dina Katabi. Delving into deep imbalanced regression. In *International Conference on Machine Learning*, pages 11842–11851. PMLR, 2021.
- [39] Liang Zeng, Lanqing Li, Ziqi Gao, Peilin Zhao, and Jian Li. Imgcl: Revisiting graph contrastive learning on imbalanced node classification. *arXiv preprint arXiv:2205.11332*, 2022.
- [40] Marina Sokolova, Nathalie Japkowicz, and Stan Szpakowicz. Beyond accuracy, f-score and roc: a family of discriminant measures for performance evaluation. In *Australasian joint conference on artificial intelligence*, pages 1015–1021. Springer, 2006.
- [41] Kay Henning Brodersen, Cheng Soon Ong, Klaas Enno Stephan, and Joachim M. Buhmann. The balanced accuracy and its posterior distribution. In *20th International Conference on Pattern Recognition, ICPR 2010, Istanbul, Turkey, 23-26 August 2010*, pages 3121–3124. IEEE Computer Society, 2010. doi: 10.1109/ICPR.2010.764. URL <https://doi.org/10.1109/ICPR.2010.764>.
- [42] Mark Davies, Michał Nowotka, George Papadatos, Nathan Dedman, Anna Gaulton, Francis Atkinson, Louisa Bellis, and John P Overington. ChEMBL web services: streamlining access to drug discovery data and utilities. *Nucleic acids research*, 43(W1):W612–W620, 2015.
- [43] Michael K Gilson, Tiqing Liu, Michael Baitaluk, George Nicola, Linda Hwang, and Jenny Chong. Bindingdb in 2015: a public database for medicinal chemistry, computational chemistry and systems pharmacology. *Nucleic acids research*, 44(D1):D1045–D1053, 2016.
- [44] Arkadiusz Z Dudek, Tomasz Arodz, and Jorge Gálvez. Computational methods in developing quantitative structure-activity relationships (qsar): a review. *Combinatorial chemistry & high throughput screening*, 9(3):213–228, 2006.
- [45] Bowen Liu, Bharath Ramsundar, Prasad Kawthekar, Jade Shi, Joseph Gomes, Quang Luu Nguyen, Stephen Ho, Jack Sloane, Paul Wender, and Vijay Pande. Retrosynthetic reaction prediction using neural sequence-to-sequence models. *ACS central science*, 3(10):1103–1113, 2017.
- [46] Matthias Delange, Rahaf Aljundi, Marc Masana, Sarah Parisot, Xu Jia, Ales Leonardis, Greg Slabaugh, and Tinne Tuytelaars. A continual learning survey: Defying forgetting in classification tasks. *IEEE Transactions on Pattern Analysis and Machine Intelligence*, 2021.
- [47] Jialei Wang, Peilin Zhao, and Steven CH Hoi. Cost-sensitive online classification. *IEEE Transactions on Knowledge and Data Engineering*, 26(10):2425–2438, 2013.
- [48] Lars Ruddigkeit, Ruud Van Deursen, Lorenz C Blum, and Jean-Louis Reymond. Enumeration of 166 billion organic small molecules in the chemical universe database gdb-17. *Journal of chemical information and modeling*, 52(11):2864–2875, 2012.

- [49] Raghunathan Ramakrishnan, Pavlo O Dral, Matthias Rupp, and O Anatole Von Lilienfeld. Quantum chemistry structures and properties of 134 kilo molecules. *Scientific data*, 1(1):1–7, 2014.
- [50] Wissam Sibli, Jordan Fréry, Liyun He-Guelton, Frédéric Oblé, and Yi-Qing Wang. Master your metrics with calibration. In *International Symposium on Intelligent Data Analysis*, pages 457–469. Springer, 2020.
- [51] Nathalie Japkowicz and Shaju Stephen. The class imbalance problem: A systematic study. *Intelligent data analysis*, 6(5):429–449, 2002.
- [52] Jiawei Ren, Cunjun Yu, Xiao Ma, Haiyu Zhao, Shuai Yi, et al. Balanced meta-softmax for long-tailed visual recognition. *Advances in Neural Information Processing Systems*, 33:4175–4186, 2020.
- [53] Seulki Park, Jongin Lim, Younghun Jeon, and Jin Young Choi. Influence-balanced loss for imbalanced visual classification. In *Proceedings of the IEEE/CVF International Conference on Computer Vision*, pages 735–744, 2021.
- [54] Hongyi Zhang, Moustapha Cissé, Yann N. Dauphin, and David Lopez-Paz. mixup: Beyond empirical risk minimization. In *6th International Conference on Learning Representations, ICLR 2018, Vancouver, BC, Canada, April 30 - May 3, 2018, Conference Track Proceedings*. OpenReview.net, 2018. URL <https://openreview.net/forum?id=r1Ddp1-Rb>.
- [55] Hsin-Ping Chou, Shih-Chieh Chang, Jia-Yu Pan, Wei Wei, and Da-Cheng Juan. Remix: rebalanced mixup. In *European Conference on Computer Vision*, pages 95–110. Springer, 2020.
- [56] Yin-Yin He, Jianxin Wu, and Xiu-Shen Wei. Distilling virtual examples for long-tailed recognition. In *Proceedings of the IEEE/CVF International Conference on Computer Vision*, pages 235–244, 2021.
- [57] Han-Jia Ye, Hong-You Chen, De-Chuan Zhan, and Wei-Lun Chao. Identifying and compensating for feature deviation in imbalanced deep learning. *CoRR*, abs/2001.01385, 2020. URL <http://arxiv.org/abs/2001.01385>.
- [58] Bingyi Kang, Saining Xie, Marcus Rohrbach, Zhicheng Yan, Albert Gordo, Jiashi Feng, and Yannis Kalantidis. Decoupling representation and classifier for long-tailed recognition. In *8th International Conference on Learning Representations, ICLR 2020, Addis Ababa, Ethiopia, April 26-30, 2020*. OpenReview.net, 2020. URL <https://openreview.net/forum?id=r1gRTCvFvB>.
- [59] Boyan Zhou, Quan Cui, Xiu-Shen Wei, and Zhao-Min Chen. Bbn: Bilateral-branch network with cumulative learning for long-tailed visual recognition. In *Proceedings of the IEEE/CVF conference on computer vision and pattern recognition*, pages 9719–9728, 2020.
- [60] Linchao Zhu and Yi Yang. Inflated episodic memory with region self-attention for long-tailed visual recognition. In *Proceedings of the IEEE/CVF Conference on Computer Vision and Pattern Recognition*, pages 4344–4353, 2020.
- [61] Thomas N Kipf and Max Welling. Semi-supervised classification with graph convolutional networks. *arXiv preprint arXiv:1609.02907*, 2016.
- [62] Minjie Wang, Da Zheng, Zihao Ye, Quan Gan, Mufei Li, Xiang Song, Jinjing Zhou, Chao Ma, Lingfan Yu, Yu Gai, Tianjun Xiao, Tong He, George Karypis, Jinyang Li, and Zheng Zhang. Deep graph library: A graph-centric, highly-performant package for graph neural networks. *arXiv preprint arXiv:1909.01315*, 2019.
- [63] David Rogers and Mathew Hahn. Extended-connectivity fingerprints. *J. Chem. Inf. Model.*, 50(5):742–754, 2010. doi: 10.1021/ci100050t. URL <https://doi.org/10.1021/ci100050t>.
- [64] David Weininger. Smiles, a chemical language and information system. 1. introduction to methodology and encoding rules. *Journal of chemical information and computer sciences*, 28(1):31–36, 1988.

- [65] David S Wishart, Yannick D Feunang, An C Guo, Elvis J Lo, Ana Marcu, Jason R Grant, Tanvir Sajed, Daniel Johnson, Carin Li, Zinat Sayeeda, et al. Drugbank 5.0: a major update to the drugbank database for 2018. *Nucleic acids research*, 46(D1):D1074–D1082, 2018.
- [66] Nitesh V Chawla, Kevin W Bowyer, Lawrence O Hall, and W Philip Kegelmeyer. Smote: synthetic minority over-sampling technique. *Journal of artificial intelligence research*, 16: 321–357, 2002.
- [67] Guy W Bemis and Mark A Murcko. The properties of known drugs. 1. molecular frameworks. *Journal of medicinal chemistry*, 39(15):2887–2893, 1996.
- [68] Tsung-Yi Lin, Priya Goyal, Ross Girshick, Kaiming He, and Piotr Dollár. Focal loss for dense object detection. In *Proceedings of the IEEE international conference on computer vision*, pages 2980–2988, 2017.
- [69] Xiaotian Han, Zhimeng Jiang, Ninghao Liu, and Xia Hu. G-mixup: Graph data augmentation for graph classification. *CoRR*, abs/2202.07179, 2022. URL <https://arxiv.org/abs/2202.07179>.
- [70] Vikas Verma, Alex Lamb, Christopher Beckham, Amir Najafi, Ioannis Mitliagkas, David Lopez-Paz, and Yoshua Bengio. Manifold mixup: Better representations by interpolating hidden states. In *International Conference on Machine Learning*, pages 6438–6447. PMLR, 2019.

A Key Information about ImDrug

A.1 Dataset Documentation

For each dataset, we provide the corresponding description which includes data statistics, data source, unit, and references. Please refer to Appendix D for more details for all 11 datasets. We host the ImDrug datasets at https://drive.google.com/drive/folders/16dSuqq-Fh6iGqjPL1phtQT3C_K70cCfK?usp=sharing, and the data is instantly accessible in human-readable form without featurization.

A.2 Intended Uses

ImDrug is intended for researchers in biomedical, machine learning, and data science to facilitate interdisciplinary research for AI-aided Drug Discovery (AIDD) and deep imbalanced learning.

A.3 Hosting and Maintenance Plan

The ImDrug codebase is hosted and version-tracked via GitHub and it will be permanently available under the link <https://github.com/DrugLT/ImDrug>. All of the datasets are hosted at https://drive.google.com/drive/folders/16dSuqq-Fh6iGqjPL1phtQT3C_K70cCfK?usp=sharing for public access and download.

ImDrug is a community-driven and open-source initiative. Our core development team will be committed to the maintenance and development of the benchmarks and datasets in the next five years at minimum. We plan to grow ImDrug by introducing new learning tasks, datasets, novel baselines, competitive backbones, and leaderboards. We welcome external contributors.

A.4 Licensing

ImDrug codebase is under the GNU General Public License v3.0. For individual dataset usage, please refer to the dataset license found in the website.

A.5 Author Statement

We the authors bear all responsibility in case of violation of rights.

A.6 Computing Resources

We use a computing server with NVIDIA Tesla V100 GPUs (32GB) and Inter(R) Xeon(R) CPUs for all empirical experiments in this paper. Each trial of experiment is run on 1 V100 GPU and 8 CPU cores in the docker image built by the docker file in <https://github.com/DrugLT/ImDrug>. For more detailed information, please refer to Appendix G.3.

A.7 Limitations

ImDrug includes commonly-used methods and datasets targeted at the intersection of imbalanced learning and AIDD, which make up the proposed emerging cross-discipline. However, ImDrug is an ongoing effort and we strive to continuously include more novel baselines that are not only explored in the field of Computer Vision. In addition, more new datasets and tasks for AIDD will also be included as follow-up work, such as the molecule generation tasks involving de novo drug design and retrosynthesis.

A.8 Potential Negative Societal Impacts

AIDD is an emerging area of research with high potential to revolutionize the pharmaceutical industry by expediting the development of safe and effective drugs. Our proposed ImDrug benchmark does not involve human subjects research or any personally identifiable information. However, for adaptation of some of the imbalanced learning baselines originally proposed in Computer Vision to the AIDD domain, we choose certain drug/protein encodings and model backbones which may not realize their

full potential due to the lack of best practices. Moreover, even though we tried to make the datasets as comprehensive as possible, their current form in limited scale and scope are likely to fall short in representing some of the real-world distributions and scenarios. Being aware of these limitations, we encourage the users and followers of this work to explore better implementation protocols, and in the mean time the datasets and trained models should be used with caution especially when applied to real-world problems.

B Theoretical Proofs

Theorem B.1. *Let Rec_k and $Prec_k$ denote the recall and balanced precision for class k . Given a trained predictor, the evaluated balanced F1 score*

$$\text{Balanced-F1} := \frac{1}{K} \sum_{k=1}^K \frac{2 \times Rec_k \times Prec_k}{Rec_k + Prec_k} \quad (4)$$

is invariant on any test set whose samples of each class are drawn i.i.d from a fixed distribution.

Proof. We start by formalizing Def. 1 from a probabilistic view. Consider the test set $\{x_i, y_i\}_{i=1}^n$ as n i.i.d draws of random variables $x \in \mathcal{X}$ and $y \in \mathcal{Y}$ from the distribution $P(x)$ and $P(y|x)$ respectively. And the trained classifier $g : \mathcal{X} \rightarrow \mathcal{Y}$ makes the corresponding set of predictions $\{\hat{y}_i = g(x_i)\}_{i=1}^n$. Then the conventional one-vs-all recall $C\text{-}Rec_k$ and precision $C\text{-}Prec_k$ for class k follow

$$C\text{-}Rec_k = \frac{\mathbb{E}[\sum_{i=1}^n \mathbb{1}(y_i = k, \hat{y}_i = k)]}{\mathbb{E}[\sum_{i=1}^n \mathbb{1}(y_i = k)]} = \frac{P(\hat{y} = k, y = k)}{P(y = k)} = \frac{P(\hat{y} = k|y = k)P(y = k)}{P(y = k)} \quad (5)$$

$$C\text{-}Prec_k = \frac{\mathbb{E}[\sum_{i=1}^n \mathbb{1}(y_i = k, \hat{y}_i = k)]}{\mathbb{E}[\sum_{i=1}^n \mathbb{1}(\hat{y}_i = k)]} = \frac{P(\hat{y} = k, y = k)}{P(\hat{y} = k)} = \frac{P(\hat{y} = k|y = k)P(y = k)}{P(\hat{y} = k)} \quad (6)$$

Note that $C\text{-}Rec_k \equiv Rec_k$. Moreover, the balanced precision for class k , as in Eqn 2, can be written as

$$Prec_k = \frac{\mathbb{E}[\sum_{i=1}^n \mathbb{1}(y_i = k, \hat{y}_i = k)]}{\mathbb{E}[\sum_{i=1}^n \mathbb{1}(y_i = k, \hat{y}_i = k) + \sum_{j \neq k} \sum_{i=1}^n \pi_{jk} \mathbb{1}(y_i = j, \hat{y}_i = k)]} \quad (7)$$

$$= \frac{P(\hat{y} = k|y = k)P(y = k)}{\int_{y'} \pi_{y'k} P(\hat{y} = k, y') dy'} \quad (8)$$

$$= \frac{P(\hat{y} = k|y = k)P(y = k)}{\int_{y'} P(\hat{y} = k|y = y')P(y = y') \times \frac{P(y=k)}{P(y=y')} dy'} \quad (9)$$

$$= \frac{P(\hat{y} = k|y = k)}{\int_{y'} P(\hat{y} = k|y = y') dy'} \quad (10)$$

where to derive Eqn. 9, we use the fact that $\forall j, k \in \mathcal{Y}, \pi_{jk} = n_k/n_j = P(y = k)/P(y = j)$. We now proceed by proving the following lemma:

Lemma B.1. *The conditional probabilities $P(\hat{y} = k|y = k)$ and $P(\hat{y} = k|y = y')$ are invariant/constant regardless of the dataset distribution $P(x)$ and $P(y)$, assuming the samples of each class are drawn i.i.d from a fixed distribution, $P(x|y)$.*

Proof. We write $P(\hat{y} = k|y = k)$ and $P(\hat{y} = k|y = y')$ as the marginal likelihood functions of x :

$$P(\hat{y} = k|y = k) = \int_x P(\hat{y} = k|x)P(x|y = k)dx \quad (11)$$

$$P(\hat{y} = k|y = y') = \int_x P(\hat{y} = k|x)P(x|y = y')dx \quad (12)$$

Note that given x and the trained classifier g , the probability $P(\hat{y} = k|x) = P(g(x) = k|x) \propto \delta(g(x), k)$ is a fixed Dirac delta function. Additionally, since the conditional distribution $P(x|y)$ is assumed to be fixed for all $y \in \mathcal{Y}$, the integrand of the RHS of Eqn. 11 and 12 are constant regardless of the dataset distribution $P(x)$ and $P(y)$, so are the LHS. This completes the proof. \square

With Lemma. B.1, evidently both the numerator and denominator of the RHS of Eqn. 10 are invariant regardless of the dataset distribution $P(x)$ and $P(y)$. This proves that the conventional recall in Eqn. 5, the balanced precision in Eqn. 10 and the proposed balanced F1 score in Eqn. 4 are all invariant/constant under any dataset distribution. In other words, given a trained classifier, the proposed balanced metrics of ImDrug provide unbiased estimate of its multi-class classification efficacy on any imbalanced test set. \square

C Documentation and Usages of the ImDrug Benchmark

The source code of ImDrug is available at <https://github.com/DrugLT/ImDrug>. The datasets in ImDrug are hosted at https://drive.google.com/drive/folders/16dSuqq-Fh6iGqjPL1phtQT3C_K70cCfK?usp=sharing. ImDrug is intended for comprehensive comparison among imbalanced learning methods. All necessary configurations for training and evaluation are stored as a JSON dictionary file following a fixed format. Listing 1 provides a simple example, which integrates all of the steps including dataset curation, dataset loading, and algorithm configurations in just a few lines of code.

```
{
  "dataset": {
    "drug_encoding": "Transformer",
    "protein_encoding": "Transformer",
    "tier1_task": "single_pred",
    "tier2_task": "ADME",
    "dataset_name": "BBB-Martins",
    "split": {
      "method": "standard",
      "by_class": false
    }
  },
  "loss": {
    "type": "CrossEntropy"
  },
  "train": {
    "batch_size": 128,
    "combiner": {
      "type": "bbn_mix"
    },
    optimizer=dict(
      type='ADAM',
      lr=1e-3,
      momentum=0.9,
      wc=2e-4,
    ),
    two_stage=dict(
      drw=False,

```

```

        drs=False,
        start_epoch=10,
    )
},
"setting": {
    "type": "LT Classification",
    "num_class": 10
},
"use_gpu": true
}

```

Listing 1: Algorithm configuration example.

Note that each configuration in the JSON file can be chosen as follows:

- **"drug_encoding"**: ["Morgan", "Pubchem", "Daylight", "rdkit_2d_normalized", "ESPF", "CNN", "CNN_RNN", "Transformer", "MPNN", "ErG", "DGL_GCN", "DGL_NeuralFP", "DGL_AtteniveFP", "DGL_GIN_AttrMasking", "DGL_GIN_ContextPred"]
- **"protein_encoding"**: ["AAC", "PseudoAAC", "Conjoint_triad", "Quasi-seq", "ESPF", "CNN", "CNN_RNN", "Transformer"]
- **"tier1_task"**: ["single_pred", "multi_pred"], both are applicable for hybrid prediction.
- **"tier2_task"**: ["ADME", "TOX", "QM", "HTS", "Yields", "DTI", "DDI", "Catalyst", "React-Type"]
- **"dataset_name"**: ["BBB_Martins", "Tox21", "HIV", "QM9", "USPTO-50K", "USPTO-Catalyst", "USPTO-1K-TPL", "USPTO-500-MT", "USPTO-Yields", "SBAP", "BindingDB_Kd"]
- **"split.method"**: ["standard", "random", "scaffold", "time", "combination", "group", "open-random", "open-scaffold", "open-time", "open-combination", "open-group"]
- **"setting.type"**: ["Imbalanced Classification", "LT Classification", "Imbalanced Regression", "Open LT"]

We also store the filtered data file without featurization for easy access in a human-readable form (*e.g.*, EXECL file). In addition, guidance for training and evaluation on a new dataset is described in the README.md file of the Github repository. The entries of 'dataset' in the JSON dictionary specify the elements of the three-level hierarchical design for datasets described in Sec. 3.1.1.

D Datasets

In this section, we give a description of the datasets we used in ImDrug. As shown in Table 5, ImDrug consists of 11 imbalanced drug datasets, 8 task types, and 6 data split functions. In what follows, we briefly introduce these datasets followed by their task types.

D.1 Datasets Descriptions

ImDrug.BBB_Martins is a binary classification dataset [6]. Given a drug SMILES string, the task is to predict the activity of the blood-brain barrier (BBB). It contains 1,975 entities, each consisting of the drug name, the drug SMILES string, and a binary label indicating whether this drug can penetrate the blood-brain barrier. The recommended setting of this dataset is imbalanced classification.

ImDrug.Tox21 is a binary classification dataset [20]. Given a drug SMILES string, the task is to predict the toxicity in one of 12 quantitative high throughput screening (qHTS) assays. It contains 7,831 entities, each consisting of the drug ID, the drug SMILES string, and 12 binary labels called NR-AR, NR-AR-LBD, NR-AhR, NR-Aromatase, NR-ER, NR-ER-LBD, NR-PPAR-gamma, SR-ARE, SR-ATAD5, SR-HSE, SR-MMP, SR-p53. The recommended setting of this dataset is imbalanced classification.

ImDrug.HIV is a binary classification dataset [6]. Given a drug SMILES string, the task is to predict this drug's activity against the HIV virus. It contains 41,127 entities, each consisting of the drug ID, the drug SMILES string, and a binary label indicating the activity of this drug against HIV.

ImDrug.QM9 is a regression dataset [48, 49]. Given a drug 3D Coulomb matrix, the task is to predict 12 drug properties. It contains 133,885 entities, each consisting of the drug ID, the drug SMILES string, the 3D coordinates of each atom, and 12 regression labels called *Mu*, *Alpha*, *Homo*, *Lumo*, *Gap*, *R2*, *Zpve*, *Cv*, *U0*, *U298*, *H298*, *G298*. The recommended setting of this dataset is imbalanced regression.

ImDrug.SBAP is a binary classification dataset. Given the amino acid sequence and the drug SMILES string, the task is to predict binding affinity between them. It contains 32,140 entities, each consisting of the drug ID, the drug SMILES string, the amino acid sequence, the protein ID, and a binary label representing binding affinity. It was extracted from the BindingDB [20] by DrugOOD [21] for the interaction prediction task. The recommended setting of this dataset is imbalanced classification.

ImDrug.USPTO-Catalyst is a multi-class classification dataset. Given the set of reactants and products, the task is to predict the catalyst type. It contains 721,799 entities, each consisting of the reactant ID, the reactant SMILES string, the product ID, the product SMILES string, and the catalyst type. It was derived from the USPTO database by TDC [20] for the catalyst prediction task. The recommended settings of this dataset are LT classification and Open LT.

ImDrug.USPTO-1K-TPL is a multi-class classification dataset. Given a reaction SMILES string, the task is to predict the reaction type. It contains 445,115 entities, each consisting of the reaction SMILES string, and the reaction type. It was collated from the USPTO dataset by this work [10] for the reaction type classification task. The recommended settings of this dataset are LT classification and Open LT.

ImDrug.USPTO-Yields is a regression dataset. Given the set of reactants and products, the task is to predict the yields. It contains 853,638 entities, each consisting of the reaction SMILES string, and the reaction yields. It was derived from the USPTO database by TDC [20] for the yield prediction task. The recommended setting of this dataset is imbalanced regression.

ImDrug.USPTO-500-MT has multiple reaction prediction tasks, including reaction yield prediction task, catalyst prediction task, and reaction type classification task. It contains 143,535 entities, each consisting of the reaction SMILES string, the reaction type, and the reaction yields. It was extracted from the USPTO dataset by T5Chem [11] for multiple tasks. The recommended settings of this dataset are LT classification/Open LT or imbalanced regression.

ImDrug.USPTO-50K is a multi-class classification dataset [20]. Given the reaction SMILES strings, the task is to predict the reaction type. It contains 50,016 entities, each consisting of the reaction SMILES string, and the reaction type. The recommended settings of this dataset are LT classification and Open LT.

ImDrug.DrugBank is a multi-class classification dataset. Given the SMILES strings of two drugs, the task is to predict the interaction type between them. It contains 191,808 entities, each consisting of two drugs' SMILES strings, ID, and interaction type. It was collated from FDA and Health Canada drug labels as well as from the primary literature by TDC [20] for the interaction type prediction task. The recommended settings of this dataset are LT classification and Open LT.

D.2 Imbalance Ratio

In order to better understand the imbalanced degree of datasets in ImDrug, we select 7 datasets as the representative examples, calculate their imbalance ratios, and plot their label histograms sorted by the class cardinality in decreasing order. As shown in Fig. 6, All datasets exhibit an imbalance ratio larger than 20, which indicates that the highly imbalanced property is ubiquitous among AIDD datasets. The datasets for multi-class classification (*e.g.*, USPTO-500-MT and USPTO-Catalyst) often have a higher highest imbalance ratio. For example, USPTO-Catalyst has an imbalanced ratio of 3975.86, and such an exaggerated numerical imbalance ratio value could inevitably affect the generalization ability of machine learning models.

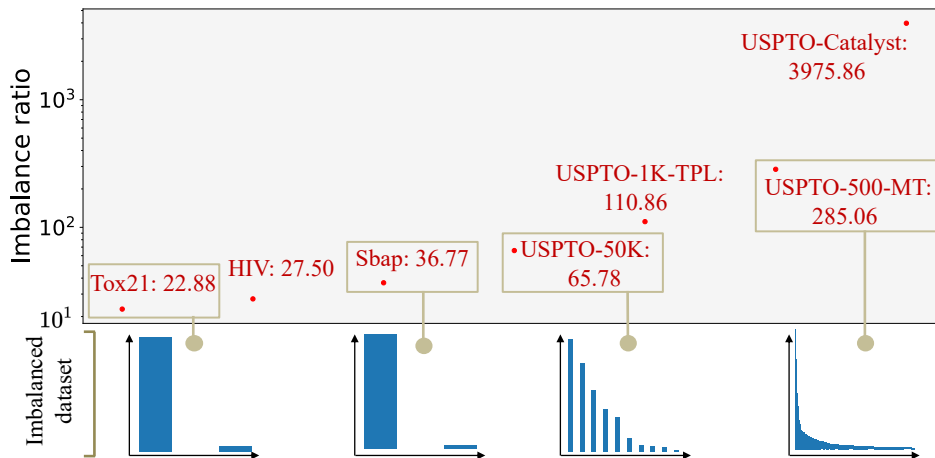


Figure 6: The comparison of datasets in imbalance ratio.

Table 5: The statistics of datasets.

Dataset	Learning Tasks	Size	# Classes	Unit	Feature	Recommended Settings
ImDrug.BBB_Martins [20]	single_pred.ADMET	1975	2	-	Seq/Graph	Imbalanced Classification
ImDrug.Tox21 [20]	single_pred.ADMET	7831	2	-	Seq/Graph	Imbalanced Classification
ImDrug.HIV [20]	single_pred.BioAct	41,127	2	-	Seq/Graph	Imbalanced Classification
ImDrug.QM9 [48, 49]	single_pred.QM	133,885	-	GHz/D ₀ ² /β ₀ ³	Coulomb	Imbalanced Regression
ImDrug.SBAP [21]	multi_pred.DTI	32,140	2	nM	Seq/Graph	Imbalanced Classification/Regression
ImDrug.USPTO-Catalyst [20]	hybrid_pred.Catalyst	721,799	888	-	Seq/Graph	LT Classification/Open LT
ImDrug.USPTO-50K [45]	hybrid_pred.ReactType	50,016	10	-	Seq/Graph	LT Classification/Open LT
ImDrug.USPTO-500-MT [11]	hybrid_pred.ReactType	143,535	500	-	Seq/Graph	LT Classification/Open LT
ImDrug.USPTO-500-MT [11]	hybrid_pred.Catalyst	143,535	27,759	-	Seq/Graph	LT Classification/Open LT
ImDrug.USPTO-500-MT [11]	hybrid_pred.Yields	143,535	-	%	Seq/Graph	Imbalanced Regression
ImDrug.USPTO-1K-TPL [10]	hybrid_pred.ReactType	445,115	1000	-	Seq/Graph	LT Classification/Open LT
ImDrug.USPTO-Yields [20]	hybrid_pred.Yields	853,638	-	%	Seq/Graph	Imbalanced Regression
ImDrug.DrugBank[20]	hybrid_pred.DDI	191,808	86	-	Seq/Graph	LT Classification/Open LT

D.3 Split Functions for Different Settings

D.3.1 Imbalanced/Long-Tailed Classification

For these two settings, the implemented data split functions make a separate splitting (one of the 6 splits specified in Fig. 1) of train/valid/test samples for each individual class, with split ratios specified in the config. The final train/valid/test sets are the union of the corresponding subset for each class.

D.3.2 Imbalanced Regression

For regression, the data split functions first create consecutive bins as "classes" of the continuous labels according to the "num_class" in Listing 1. The same procedure as in Appendix D.3.1 is applied subsequently.

D.3.3 Open LT

For Open LT, we reserve a portion of the minority classes (with ratio specified in the configuration file) as the "open set", which is added to the test set only. The same procedure as in Appendix D.3.1 is applied subsequently. This ensures that there are open classes at test time which are unseen during training/validation.

E Imbalanced Learning Baselines

In this section, we provide detailed descriptions of the imbalanced learning baselines benchmarked in ImDrug.

E.1 Baselines of Imbalanced & Long-Tailed Classification

Class Re-balancing. 4 imbalanced learning baselines are included in this category. Compared to the conventional **softmax cross-entropy loss (CE)**, **cost-sensitive loss (CS)** [51] re-weights the log likelihood of each prediction inversely proportional to its label frequency π_y . **Class-balanced loss** [34] introduces a novel concept, namely effective number, to approximate the expected sample number of each class. The re-weighting factor is given by the reciprocal of the effective number in the form of an exponential function of the training sample number, which can be applied to a normal Focal loss [68] (**CB_F**) or cross-entropy loss (**CB_CE**). **Balanced softmax** [52] (**BS**) proposes to adjust the predicted logits by label frequencies to alleviate the bias of class imbalance. **Influence-balanced training** [53] (**IB**) down-weights highly influential samples measured by the gradient magnitude at fine-tuning to smooth the decision boundary, thus mitigating over-fitting and class bias. All baselines in this family can be implemented via loss functions summarized in Table 6.

Table 6: **Summary of re-balancing losses.** z and p denote the predicted logits and the softmax probability of the sample x , with subscript y being the corresponding class label. n_y and π_y indicate the sample number and label frequency of the class y . γ and β are loss-related hyperparameters.

Losses	Formulation
Softmax loss (vanilla)	$\mathcal{L}_{CE} = -\log(p_y)$
Cost-sensitive loss [51]	$\mathcal{L}_{CS} = -\frac{1}{\pi_y} \log(p_y)$
Class-balanced focal loss [34]	$\mathcal{L}_{CB_F} = -\frac{1-\gamma}{1-\gamma^{n_y}} (1-p_y)^\beta \log(p_y)$
Class-balanced cross-entropy loss [34]	$\mathcal{L}_{CB_CE} = -\frac{1-\gamma}{1-\gamma^{n_y}} \log(p_y)$
Balanced softmax loss [52]	$\mathcal{L}_{BS} = -\log\left(\frac{\pi_y \exp(z_y)}{\sum_j \pi_j \exp(z_j)}\right)$
Influence-balanced loss [53]	$\mathcal{L}_{IB} = -\frac{1}{\pi_y \ \nabla \log(p_y)\ _1} \log(p_y)$

Information Augmentation. ImDrug benchmarks 2 data augmentation (Mixup and Remix) and 1 transfer learning (DiVE) baselines. **Mixup** [54] is a classical trick which constructs augmented data by making convex combination of two samples and their labels to improve the generalization ability of models. Specifically, Mixup is formed by the linear interpolation of two samples (x_i, y_i) and (x_j, y_j) obtained at the training data:

$$\begin{aligned}\tilde{x}^{MU} &= \lambda x_i + (1 - \lambda)x_j \\ \tilde{y}^{MU} &= \lambda y_i + (1 - \lambda)y_j,\end{aligned}\tag{13}$$

where λ is randomly sampled from the predefined beta distribution. Built upon Mixup, **Remix** [55] assigns the mixed label in favor of the minority class by providing a disproportionately higher weight to the minority class. The formulation of Remix is as below:

$$\begin{aligned}\tilde{x}^{RM} &= \lambda_x x_i + (1 - \lambda_x)x_j \\ \tilde{y}^{RM} &= \lambda_y y_i + (1 - \lambda_y)y_j,\end{aligned}\tag{14}$$

where λ_x is sampled from the beta distribution and λ_y is designed related to number of samples.

However, it is worth noticing that the conventional Mixup/Remix approach performed on the input data in the CV domain cannot be trivially applied to graph or sequence data [69] due to their non-Euclidean structures. Instead, manifold Mixup/Remix [70] which perform interpolations of hidden representations, are implemented in ImDrug.

Lastly, as a transfer learning method, **DiVE** [56] employs a class-balanced model as the teacher to generate virtual examples. By distillation, it achieves remarkable head-to-tail knowledge transfer for long-tailed learning. Supposing there are C classes in total, we define the predicted logits of the student network and teacher network in DiVE as $\mathbf{s} = (s_1, s_2, \dots, s_C)$ and $\mathbf{t} = (t_1, t_2, \dots, t_C)$ respectively. The loss function of the student network is shown below:

$$L_{KD} = -(1 - \Lambda) \sum_{k=1}^C y_k \log s_k + \Lambda \sum_{k=1}^C t_k \log \frac{t_k}{s_k},\tag{15}$$

where the hyperparameter $\Lambda \in [0, 1]$ balances the two terms.

Module Improvement. We consider 1 classifier design (CDT), 1 decoupled training (Decoupling) and 1 ensemble learning (BBN) methods. **CDT** [57] proposes to incorporate class-dependent temperatures to force minor classes to have larger decision values in the training phase, so as to compensate for the effect of feature deviation in the test data. We denote $\mathbf{w}_c^\top \mathbf{f}_\theta(x)$ as the decision values of a training instance and a_c as the temperature factor. The proposed training objective in CDT is as follows:

$$-\sum_n \log \left(\frac{\exp \left(\frac{\mathbf{w}_{y_n}^\top \mathbf{f}_\theta(x_n)}{a_{y_n}} \right)}{\sum_c \exp \left(\frac{\mathbf{w}_c^\top \mathbf{f}_\theta(x_n)}{a_c} \right)} \right), \quad (16)$$

where $c \in \{1, \dots, C\}$, $n \in \{1, \dots, N\}$, C and N denote the number of class and the number of training samples, respectively.

Decoupling [58] is the pioneering work to introduce a two-stage training scheme. It employs instance-balanced sampling for representation learning in the first stage and transitions to class-balanced sampling for training the classifier in the later stage. In a nutshell, the combined sampling method is as follows:

$$p_j^{\text{PB}}(t) = (1 - \frac{t}{T})p_j^{\text{IB}} + \frac{t}{T}p_j^{\text{CB}}, \quad (17)$$

where t is the current number of training epoch, T is the overall epoch number, p^{IB} means the instance-balanced sampling and p^{CB} means the class-balanced sampling.

BBN [59] consists of a conventional learning branch and a re-balancing branch. To handle long-tailed recognition, the predictions of two branches are dynamically combined during training, ensuring that the learning focus gradually shifts from head classes to tail classes. By using uniform and reversed samplers in the bilateral branches, two samples (x_c, y_c) and (x_r, y_r) are obtained as the input data. The output logits are as follows:

$$\mathbf{z} = \beta \mathbf{W}_c^\top \mathbf{f}_c + (1 - \beta) \mathbf{W}_r^\top \mathbf{f}_r, \quad (18)$$

where the weights \mathbf{f}_c and \mathbf{f}_r are controlled with a trade-off parameter β , \mathbf{W}_c and \mathbf{W}_r mean the classifiers of the two branches. Finally, a loss of weighted cross-entropy classification is applied as:

$$\mathcal{L} = \beta E(\hat{\mathbf{p}}, y_c) + (1 - \beta) E(\hat{\mathbf{p}}, y_r). \quad (19)$$

E.2 Baselines of Open LT & Imbalanced Regression

Open LT can be regarded as a variant of conventional long-tailed classification with unseen and out-of-distribution (OOD) tail classes in the test set. In principle, all aforementioned baselines for imbalanced classification can be seamlessly transferred to this setting. However, the extra challenge posed by the protocol requires targeted remedies to OOD generalization to achieve state-of-the-art performance. Hence ImDrug includes 2 additional baselines for Open LT. **OLTR** [33] as the seminal work in this line of research, explores the idea of feature prototypes to handle long-tailed recognition with open-set detection. For an input drug/protein, OLTR first learns the visual memory M of all the training data:

$$M = \{c_i\}_{i=1}^K, \quad (20)$$

where K is the number of training classes and c_i is the centroid of each class group. The most important part is to differentiate the samples of the training dataset from those of open-set. OLTR minimizes the distance between the v^{direct} feature vector and the discriminative centroids:

$$\gamma := \text{reachability}(v^{\text{direct}}, M) = \min_i \|v^{\text{direct}} - c_i\|_2. \quad (21)$$

IEM [60] further innovates the meta-embedding memory by a dynamical update scheme, where each class has independent memory blocks and records only the most discriminative feature prototypes. The soft attention mechanism is applied in IEM. Given a query \mathbf{q} , the output p is generated by:

$$p = \frac{\sum_i s(\mathbf{q}, \mathbf{k}_i) v_i}{\sum_i s(\mathbf{q}, \mathbf{k}_i)}, \quad (22)$$

where v_i denotes the i -th prediction score in value memory, and \mathbf{k}_i is the i -th vector of the key memory. $s(\cdot)$ denotes the similarity function that measures distances between two vectors. Another key component is the self-attention module. Define the query, key, and value as \mathbf{Q} , \mathbf{K} and \mathbf{V} respectively, the global representation for the whole feature map is as follows:

$$\text{SA}(\mathbf{Q}, \mathbf{K}, \mathbf{V}) = \text{Softmax} \left(\frac{\mathbf{Q}\mathbf{K}^\top}{\sqrt{d}} \right) \mathbf{V}, \quad (23)$$

where d is the size of input channel.

Imbalanced Regression can be reduced to conventional imbalanced classification by naively divide the continuous label space into multiple consecutive bins as classes. In this way, many baselines in Appendix E.1 can be adapted by replacing the classification head as a regression head. However, such trivial transformation undermines the intrinsic topology of labels induced by the Euclidean distance, leading to sub-optimal performance [38]. In ImDrug, we experiment with 3 extra baselines specialized at solving this particular challenge. **Focal-R** is a regression version of the focal loss proposed by Yang et al. [38], where the scaling factor is replaced by a continuous function that maps the absolute error into $[0, 1]$. Precisely, it can be expressed as:

$$\mathcal{L}_{Focal-R} = \frac{1}{n} \sum_{i=1}^n \sigma(|\beta e_i|)^\gamma e_i, \quad (24)$$

where e_i denotes the L_1 error of the i -th sample in training set, $\sigma(\cdot)$ denotes the *Sigmoid* function, and β, γ are hyperparameters.

Label Distribution Smoothing (LDS) [38] convolves a symmetric kernel with the empirical density distribution to extract a kernel-smoothed version that accounts for the overlap in the information of data samples of nearby labels. Given target values y' and any y , for $\forall y, y' \in \mathcal{Y}$, LDS indeed computes the density distribution of effective label:

$$\tilde{p}(y') \triangleq \int_{\mathcal{Y}} k(y, y') p(y) dy, \quad (25)$$

where $p(y)$ denotes the appearance number of label y in the training set, $k(\cdot, \cdot)$ denotes the kernel function (such as the Gaussian kernel function), and $\tilde{p}(y')$ denotes the effective density of label y' .

Feature Distribution Smoothing (FDS) [38] transfers the feature statistics between nearby target bins by performing distribution smoothing on the feature space, thereby calibrating the biased estimates of feature distribution, especially for underrepresented target values. Let $\tilde{\mu}_b$ and $\tilde{\Sigma}_b$ be the mean value and covariance of each bin. The smoothed version of the two statistics is as follows:

$$\tilde{\mu}_b = \sum_{b' \in \mathcal{B}} k(y_b, y_{b'}) \mu_{b'}, \quad (26)$$

$$\tilde{\Sigma}_b = \sum_{b' \in \mathcal{B}} k(y_b, y_{b'}) \Sigma_{b'}, \quad (27)$$

where \mathcal{B} means the target bins.

F Backbone models

How to effectively and efficiently represent molecules is a crucial problem in biology and chemistry. Recently, numerous efforts have since been introduced to obtain better molecular representations [63, 64, 62, 61]. In general, existing work can be divided into three main categories: conventional molecular fingerprints (Morgan [63]), string-based representations (Transformer [64]), and graph-based representations (Graph neural networks [61]). In what follows, we briefly introduce three main representative methods, followed by ablations of backbone models on USPTO-50K.

Morgan. Fingerprints is a conventional molecular representation, which applies a kernel to a molecule to generate a numerical vector. Morgan [63] is a representative fingerprint suitable for both small and large molecules by combining substructure and atom-pair concepts. Morgan is a similarity fingerprint consisting of two atom types: connectivity (element, #heavy neighbors, #Hs, charge, isotope, inRing) and chemical features (donor, acceptor, aromatic, halogen, basic, acidic). Morgan also takes into account the neighborhood of each atom within less than 3 bonds.

Transformer. The Transformer architecture has pushed the boundaries of many research domains, such as Neural Language Processing (NLP) and Computer Vision (CV). The Transformer layer mainly consists of two components: a self-attention module and a position-wise feed-forward network (FFN). We denote by $\mathbf{H} = [\mathbf{h}_1; \dots; \mathbf{h}_n] \in \mathbb{R}^{N \times d}$ the input matrix of the self-attention module where d is the hidden dimension and \mathbf{h}_i is the embedding vector at position i . We project the input \mathbf{H}

by three learnable weight matrices $\mathbf{W}_Q \in \mathbb{R}^{d \times d_Q}$, $\mathbf{W}_K \in \mathbb{R}^{d \times d_K}$, and $\mathbf{W}_V \in \mathbb{R}^{d \times d_V}$ and obtain the corresponding representations \mathbf{Q} , \mathbf{K} , and \mathbf{V} respectively. Overall, the self-attention module is calculated as follows:

$$\mathbf{Q} = \mathbf{H}\mathbf{W}_Q, \quad \mathbf{K} = \mathbf{H}\mathbf{W}_K, \quad \mathbf{V} = \mathbf{H}\mathbf{W}_V, \quad (28)$$

$$\text{Att}(\mathbf{H}) = \frac{\mathbf{Q}\mathbf{K}^T}{\sqrt{d_K}}\mathbf{V},$$

where the term $\frac{\mathbf{Q}\mathbf{K}^T}{\sqrt{d_K}}$ usually measures the similarity between queries and keys. We often set $d_Q = d_K = d_V = d$ for simplicity. Typically, we employ multi-head attention layers to stabilize the learning process and enlarge the expressive power of self-attention.

Graph neural networks. Modern GNNs follows a message-passing mechanism [62]. During each message-passing iteration, a hidden embedding $\mathbf{h}_u^{(k)}$ corresponding to each node $u \in \mathcal{V}$ is updated by aggregating information from u 's neighborhood $\mathcal{N}(u)$. Graph Convolutional Networks (GCN) [61] updates the hidden embedding as

$$\mathbf{H}^{(l+1)} = \sigma\left(\hat{\mathbf{A}}\mathbf{H}^{(l)}\mathbf{W}^{(l)}\right), \quad (29)$$

where $\mathbf{H}^{(l+1)} = [\mathbf{h}_1^{(l+1)}, \dots, \mathbf{h}_n^{(l+1)}]$ is the hidden matrix of the $(l+1)$ -th layer. $\hat{\mathbf{A}} = \hat{\mathbf{D}}^{-1/2}(\mathbf{A} + \mathbf{I})\hat{\mathbf{D}}^{-1/2}$ is the re-normalization of the adjacency matrix, and $\hat{\mathbf{D}}$ is the corresponding degree matrix of $\mathbf{A} + \mathbf{I}$. $\mathbf{W}^{(l)} \in \mathbb{R}^{C_l \times C_{l-1}}$ is the filter matrix in the l -th layer with C_l referring to the size of l -th hidden layer and $\sigma(\cdot)$ is a nonlinear function, e.g., ReLU.

Table 7: Ablations of backbone models on USPTO-50K and USPTO-Catalyst. For hybrid prediction tasks/datasets, Unless otherwise specified, the training mode is single-instance prediction. USPTO-Catalyst here was formulated as multi-instance prediction.

			USPTO-50k			USPTO-Catalyst		
			Balanced-Acc	Balanced-F1	AUROC	Balanced-Acc	Balanced-F1	AUROC
Random	Baseline	Morgan	81.42 \pm 1.19	81.56 \pm 1.16	97.40 \pm 0.74	14.62 \pm 0.49	16.57 \pm 0.58	87.65 \pm 0.21
		Transformer	91.54 \pm 0.47	91.62 \pm 0.46	99.52 \pm 0.09	17.11 \pm 1.34	17.08 \pm 3.84	94.72\pm0.21
		GCN	92.23 \pm 0.87	92.20 \pm 0.90	99.76 \pm 0.06	16.33 \pm 0.56	15.85 \pm 2.15	92.81 \pm 0.41
	CB_F	Morgan	81.59 \pm 0.44	81.85 \pm 0.44	95.61 \pm 0.37	13.14 \pm 1.44	14.67 \pm 1.52	85.82 \pm 0.27
		Transformer	91.49 \pm 0.66	91.55 \pm 0.62	99.20 \pm 0.13	17.98 \pm 0.38	18.17 \pm 0.45	90.45 \pm 0.08
		GCN	93.32 \pm 0.18	93.33 \pm 0.2	99.49 \pm 0.10	21.36 \pm 0.61	23.09\pm0.72	90.56 \pm 0.10
	Mixup	Morgan	83.72 \pm 0.56	83.88 \pm 0.53	97.66 \pm 0.23	15.41 \pm 0.3	16.39 \pm 0.36	89.38 \pm 0.17
		Transformer	91.22 \pm 0.61	91.29 \pm 0.57	99.16 \pm 0.13	12.86 \pm 0.18	12.57 \pm 0.19	94.34 \pm 0.06
		GCN	95.03 \pm 0.77	95.04 \pm 0.78	99.77\pm0.03	16.95 \pm 0.56	18.69 \pm 0.69	94.11 \pm 0.09
	BBN	Morgan	83.57 \pm 1.32	83.81 \pm 1.43	97.11 \pm 0.14	18.30 \pm 0.65	21.18 \pm 0.66	83.59 \pm 0.39
		Transformer	89.51 \pm 0.81	89.61 \pm 0.77	98.41 \pm 0.46	9.71 \pm 8.32	9.03 \pm 7.83	76.53 \pm 22.26
		GCN	95.57\pm0.14	95.56\pm0.14	99.67 \pm 0.03	22.27\pm1.73	22.70\pm1.40	89.08 \pm 1.86
Standard	Baseline	Morgan	82.04 \pm 3.13	81.77 \pm 3.41	96.94 \pm 0.60	13.89 \pm 0.17	12.96 \pm 1.95	87.79 \pm 0.73
		Transformer	92.13 \pm 1.02	92.17 \pm 0.99	99.47 \pm 0.35	16.66 \pm 0.90	15.68 \pm 2.40	94.97\pm0.36
		GCN	92.15 \pm 0.88	92.15 \pm 0.87	99.54 \pm 0.12	16.33 \pm 0.56	15.85 \pm 2.15	92.81 \pm 0.41
	CB_F	Morgan	81.09 \pm 4.14	81.16 \pm 4.18	94.20 \pm 0.36	12.51 \pm 0.56	11.76 \pm 1.43	86.48 \pm 0.47
		Transformer	91.78 \pm 1.13	91.86 \pm 1.13	99.21 \pm 0.23	18.26 \pm 0.72	16.48 \pm 1.50	91.19 \pm 0.51
		GCN	94.07 \pm 1.18	94.11 \pm 1.20	99.27 \pm 0.31	21.68 \pm 0.28	20.51\pm1.93	90.82 \pm 0.40
	Mixup	Morgan	84.26 \pm 1.26	84.33 \pm 1.35	96.78 \pm 0.97	14.86 \pm 0.10	13.45 \pm 1.37	89.50 \pm 0.49
		Transformer	91.58 \pm 1.51	91.64 \pm 1.49	98.74 \pm 0.13	12.41 \pm 0.17	10.45 \pm 0.89	94.90 \pm 0.27
		GCN	95.21 \pm 0.37	95.19 \pm 0.33	99.65 \pm 0.29	16.62 \pm 1.03	15.50 \pm 2.28	94.38 \pm 0.28
	BBN	Morgan	85.26 \pm 2.78	85.31 \pm 2.89	97.55 \pm 0.61	17.04 \pm 1.69	16.5 \pm 3.40	86.30 \pm 0.37
		Transformer	88.77 \pm 2.81	89.02 \pm 2.68	98.63 \pm 0.18	14.25 \pm 2.14	12.19 \pm 2.91	91.36 \pm 1.12
		GCN	96.23\pm1.35	96.25\pm1.32	99.75\pm0.23	21.79\pm0.96	20.61\pm1.69	91.18 \pm 1.70

Ablation study. In order to compare the three aforementioned backbone models, we conduct experiments on USPTO-50K using the random and standard split. As shown in Table 7, we find that data-driven molecular representation methods (*i.e.*, Transformer and GCN) significantly outperform the conventional molecular representation methods (*i.e.*, Morgan). Specifically, the absolute improvement over the GCN baseline model and Morgan baseline model is about 20 percent in terms of *Balanced-Acc*, *Balanced-F1*, and *AUROC*. This suggests that the performance of conventional molecular representation methods will be largely hindered due to the enormous magnitude of possible stable chemical compounds. Moreover, the GCN model can better preserve the rich structural information of molecules and surpass the Transformer models by a large margin.

G Implementation Details

G.1 Evaluation Metrics

In this section, we give a description of 23 evaluation metrics we used in ImDrug, including 6 metrics for the regression task, 8 metrics for the binary classification task, 3 multi-class classification metrics, and 6 metrics for the molecule generation task. Besides, we provide 2 novel imbalanced learning metrics, *i.e.*, Balanced Accuracy and Balanced F1.

G.1.1 Regression

1) *Mean Squared Error (MSE)* computes the mean squared error. It is defined as

$$MSE(y, \hat{y}) = \frac{1}{n} \sum_{i=1}^n (y_i - \hat{y}_i)^2, \quad (30)$$

where \hat{y}_i is the predicted value of i -th sample, y_i is the corresponding true value, and n is the number of samples.

2) *Root-Mean Squared Error (RMSE)* computes the root mean squared error. It is defined as

$$RMSE(y, \hat{y}) = \sqrt{\frac{1}{n} \sum_{i=1}^n (y_i - \hat{y}_i)^2}, \quad (31)$$

where \hat{y}_i is the predicted value of i -th sample, y_i is the corresponding true value, and n is the number of samples.

3) *Mean Absolute Error (MAE)* computes mean absolute error. It is defined as

$$MAE(y, \hat{y}) = \frac{1}{n} \sum_{i=1}^n |y_i - \hat{y}_i|, \quad (32)$$

where \hat{y}_i is the predicted value of i -th sample, y_i is the corresponding true value, and n is the number of samples.

4) *Coefficient of Determination (R^2)* computes the coefficient of determination, usually denoted as R^2 . It is defined as

$$R^2(y, \hat{y}) = 1 - \frac{\sum_{i=1}^n (y_i - \hat{y}_i)^2}{\sum_{i=1}^n (y_i - \bar{y})^2}, \quad (33)$$

where $\bar{y} = \frac{1}{n} \sum_{i=1}^n y_i$.

5) *Pearson Correlation Coefficient (PCC)* computes the amount of linear correlations between the true values and the predicted values. It is defined as

$$PCC = \frac{C_{1,0}}{\sqrt{C_{1,1} * C_{0,0}}}, \quad (34)$$

where C is the covariance matrix of two input sequences.

6) *Spearman Correlation Coefficient* computes a Spearman correlation coefficient with associated p-value. It is defined as

$$\rho_{R(y), R(\hat{y})} = \frac{\text{cov}(R(y), R(\hat{y}))}{\sigma_{R(y)} \sigma_{R(\hat{y})}}, \quad (35)$$

where ρ denotes the usual Pearson correlation coefficient, but applied to the rank variables, $\text{cov}(R(y), R(\hat{y}))$ is the covariance of the rank variables, $\sigma_{R(y)}$ and $\sigma_{R(\hat{y})}$ are the standard deviations of the rank variables.

G.1.2 Binary Classification

1) *ROC-AUC* computes Area Under the Receiver Operating Characteristic Curve from prediction scores.

2) *PR-AUC/AUPRC* computes the Area Under the Precision-Recall Curve from prediction scores.

- 3) *Accuracy* computes the accuracy score, either the fraction (default) or the count (normalize=False) of correct predictions. It is defined as

$$Accuracy(y, \hat{y}) = \frac{1}{n} \sum_{i=1}^n \mathbf{1}(\hat{y}_i = y_i), \quad (36)$$

where \hat{y}_i is the predicted value of i -th sample, y_i is the corresponding true value, and n is the number of samples.

- 4) *Precision* computes the precision score. It is defined as

$$Precision = \frac{tp}{tp + fp}, \quad (37)$$

where tp is the number of true positives and fp the number of false positives.

- 5) *Recall* computes the recall score. It is defined as

$$Recall = \frac{tp}{tp + fn}, \quad (38)$$

where tp is the number of true positives and fn the number of false negatives.

- 6) *F1* computes the F1 score, also known as balanced F-score or F-measure. It is defined as

$$F1 = \frac{2 \times Precision \times Recall}{Precision + Recall}. \quad (39)$$

- 7) *Precision at Recall of K* computes the precision value at the minimum threshold where recall has K .

- 8) *Recall at Precision of K* computes the recall value at the minimum threshold where precision has K .

G.1.3 Multi-class Classification

- 1) *Micro-F1*, *Micro-Precision*, *Micro-Recall*, *Accuracy* computes metrics globally by counting the total true positives, false negatives, and false positives.
- 2) *Macro-F1* computes metrics for each label and finds their unweighted mean. This does not take label imbalance into account.
- 3) *Cohen's Kappa (Kappa)* is a statistic that measures inter-annotator agreement. It is defined as

$$\kappa = \frac{p_o - p_e}{1 - p_e}, \quad (40)$$

where p_o is the empirical probability of agreement on the label assigned to any sample (the observed agreement ratio), and p_e is the expected agreement when both annotators assign labels randomly. p_e is estimated using a per-annotator empirical prior over the class labels.

G.1.4 Molecule Generation Metric

- 1) *Diversity* evaluates the internal diversity of a set of molecules.
- 2) *KL divergence* evaluates the KL divergence of the set of generated smiles using the list of training smiles as reference.
- 3) *Frechet ChemNet Distance (FCD)* evaluates the FCD distance between generated smiles set and training smiles set.
- 4) *Novelty* evaluates the novelty of set of generated smiles using list of training smiles as reference. It is defined as

$$Novelty = \frac{|S_{gen} \setminus S_{train}|}{|S_{gen}|}, \quad (41)$$

where S_{gen} is the set of generated SMILES strings, S_{train} is the set of SMILES strings for training, and \setminus means set minus.

- 5) *Validity* evaluates the chemical validity of a single molecule in terms of SMILES string. It is defined as

$$Validity = \frac{|valid(S)|}{|S|}, \quad (42)$$

where S is the set of SMILES strings, $valid(\cdot)$ removes the SMILES strings failed to be converted as molecules.

- 6) *Uniqueness* evaluates the uniqueness of a list of SMILES string, i.e., the fraction of unique molecules among a given list. It is defined as

$$Uniqueness = \frac{|unique(S)|}{|S|}, \quad (43)$$

where S is the set of SMILES strings, $unique(\cdot)$ removes the SMILES strings converted to the same molecules as the others.

G.1.5 Novel Imbalanced Learning Metrics

Balanced-Acc and *Balanced-F1* are two proposed imbalanced learning metrics, which are introduced in Sec. 3.2 of the main text. We provide a script³ in our GitHub repo to demonstrate the three key advantages of our proposed balanced metrics:

1. They are the only metrics that are invariant to the label distribution of test sets.
2. Due to 1, they are the only metrics that can be tested without loss of fairness on much larger, imbalanced test sets, resulting in significantly lower variance/uncertainty.
3. Due to 2, the lower variance/uncertainty means that when ranking different models, the proposed metrics provide better statistical significance and discriminative power, which is evident in our pairwise t-tests.

G.2 Encoding Featurizers

To encourage a diverse development environment, our released benchmark provides 23 featurizers at the bottom level. In what follows, we provide a detailed description of the 23 featurizers for data processing utilities, involving 15 featurizers customized for drugs and 8 featurizers customized for proteins.

G.2.1 Drug featurizers.

- 1) *Morgan* encodes SMILES strings of drugs into extended-connectivity fingerprints for representing quantitative structure-activity relationship (QSAR).
- 2) *Pubchem* encodes SMILES strings of drugs into Pubchem substructure-based fingerprints for representing chemical structures.
- 3) *Daylight* encodes SMILES strings of drugs into Daylight-type fingerprints for representing all possible linkage pathways for drugs to reach a given length.
- 4) *RDKit_2d_normalized* encodes SMILES strings of drugs into normalized descriptors by applying a series of normalization transforms to correct functional groups and recombine charges.
- 5) *ESPF* encodes SMILES strings of drugs into explainable substructure partition fingerprints which can cleverly partition the input drug to discrete pieces of moderate-sized sub-structures.
- 6) *CNN* encodes SMILES strings of drugs with Convolutional Neural Networks (CNN) for automatically obtaining low-dimensional representations of input drugs.
- 7) *CNN_RNN* encodes SMILES strings of drugs with a Gated Recurrent Unit (GRU) or Long Short-Term Memory (LSTM) on top of CNN, which can model the nonlinear order of SMILES strings.
- 8) *Transformer* encodes SMILES strings of drugs with the transformer on ESPF.
- 9) *MPNN* encodes SMILES strings of drugs with message passing neural networks, containing the message passing and readout components.

³<https://github.com/DrugLT/ImDrug/blob/main/rebuttal.ipynb>

- 10) *ErG* encodes SMILES strings of drugs with extended reduced graphs for obtaining the pharmacophore-type node descriptions of drugs.
- 11) *DGL_GCN* first transforms SMILES strings of drugs to molecular graphs based on the DGL⁴ library. DGL graphs are then modeled with Graph Convolutional Networks (GCN) to aggregate information from the neighbor nodes.
- 12) *DGL_NeuralFP* first transforms SMILES strings of drugs to molecular graphs based on the DGL library and then constructs non-linear fingerprints with neural networks.
- 13) *DGL_AttentiveFP* first transforms SMILES strings of drugs to molecular graphs based on the DGL library and then learns interpretable representations of drugs with a graph attentive mechanism.
- 14) *DGL_GIN_AttrMasking* first transforms SMILES strings of drugs to molecular graphs based on the Graph Isomorphism Network (GIN) and then adapts the pretraining strategy to molecule graph with attribute masking.
- 15) *DGL_GIN_ContextPred* first transforms SMILES strings of drugs to molecular graphs based on the GIN model and then adapts the pretraining strategy to molecule graph with context prediction.

G.2.2 Protein Featurizer

- 1) *AAC* directly encodes an amino acid sequence for representing a target protein.
- 2) *PseudoAAC* encodes a pseudo-amino acid sequence for representing a target protein.
- 3) *Conjoint_triad* encodes the conjoint triad features for representing a protein. *Conjoint_triad* first clusters 20 amino acids into seven classes and then regards any three consecutive amino acids into a unit.
- 4) *Quasi-seq* represents a target protein by deriving the quasi-sequence order descriptor from the physicochemical distance matrix between the 20 amino acids.
- 5) *ESPF* encodes an amino acid sequence into an explainable substructure partition, which can cleverly partition the input protein into discrete pieces of moderate-sized sub-structures.
- 6) *CNN* encodes an amino acid sequence of a target protein with CNN for automatically obtaining low-dimensional representations of input drugs.
- 7) *CNN_RNN* encodes an amino acid sequence of a target protein with a GRU or LSTM on top of CNN, which can model the nonlinear order of the amino acid sequence.
- 8) *Transformer* encodes an amino acid sequence of a target protein with transformer on ESPF.

G.3 Hyperparameters and Infrastructure

For the reproducibility of our proposed benchmark, we list the hyperparameters used in the ImDrug benchmark. We mainly follow the official hyperparameters based on the DeepPurpose⁵ framework. Specifically, we uniformly sample batches of size 128 for training with the maximum number of epochs 200. We adopt an ADAM optimizer with a learning rate of $1e-3$. The value of momentum and weight decay of ADAM is set to 0.9 and $2e-4$ respectively. We use the linear warmup strategy to schedule the learning rate where we linearly increase the learning rate from a low rate to a constant rate thereafter. We set the warmup epoch and the linear factor 0.01 and 20 respectively.

Our implementation of ImDrug benchmark is based on the DeepPurpose framework. We implement GNN models based on the DGL⁶ library. We use GCN as the representative GNN model in our experiments. The GCN model consists of three layers, whose hidden feature dimension is 64. The detailed hyperparameters of each backbone model are listed as follows:

- DGL_GCN
 - Dimension of the hidden layer: 64
 - Number of layers: 3
 - Non-linearity function: ReLU

⁴<https://github.com/dmlc/dgl>

⁵<https://github.com/kexinhuang12345/DeepPurpose>

⁶<https://github.com/dmlc/dgl>

- Morgan
 - Dimension of the hidden layer: [1024, 256, 64],
- Transformer
 - Dimension of feature embedding: 128,
 - Number of attention heads: 8,
 - Number of layers: 8,
 - Dropout rate: 0.1,
 - Dropout rate in the attention layers: 0.1,
 - Dropout rate in the hidden layers: 0.1,

Moreover, all experiments are conducted with the following experimental settings:

- Operating system: Linux Red Hat 4.8.2-16
- CPU: Intel(R) Xeon(R) Platinum 8255C CPU @ 2.50GHz
- GPU: NVIDIA Tesla V100 SXM2 32GB
- Software versions: Python 3.8.10; Pytorch 1.9.0+cu102; Numpy 1.20.3; SciPy 1.7.1; Pandas 1.3.4; scikit-learn 1.0.1; PyTorch-geometric 2.0.2; DGL 0.7.2; Open Graph Benchmark 1.3.2

H More Results on Other Evaluation Metrics

For a comprehensive evaluation, we adopt widely-used metrics for imbalanced datasets including AUPRC, Kappa, MCC, Weighted-F1, Micro-F1, and Macro-F1. As shown in Table 8, we compare different deep imbalanced learning methods under the random and standard split on four datasets including HIV, SBAP, USPTO-50K, and DrugBank.

We observe that results in Table 8 are relatively consistent with those in Table 2 and moreover the proposed balanced-Acc and balanced-F1 have two clear advantages in label distribution shift invariance and the significance of evaluation. First, the proposed balanced metrics are invariant to label distribution shift and exhibit a good Pearson’s R correlation (up to 0.9 in average) between random and standard splits on four datasets. AUPRC has the highest Pearson’s R correlation among the rest metrics, which is 0.7346 in average. Then we explore a key property, p-value, on all metrics to quantify the ability for evaluation significance. Simply put, a smaller p-value represents stronger evidence in favor of the alternative hypothesis. On all four datasets, the proposed balanced metrics achieve consistently lower p-values. On average, p-values of balanced-Acc and balanced-F1 are respectively 2.47% and 1.01% lower than those of AUPRC.

I Learning Curves

We show an example of learning curves in Figure 7 to verify the absence of overfitting issues. The following observations for training on HIV dataset are made: (1) The train/validation curves are stable, especially, after 50 epochs, the curves of train and validation loss are highly matched, indicating the basic ability for GCN to stabilize the imbalanced learning; (2) The balanced-Acc of validation data shows an upward trend as the epoch increases and at the best epoch, the final validation balanced-Acc is only 3.26% lower than the training balanced-Acc, suggesting no risk of overfitting.

Table 8: **Results for random and standard splits on 4 ImDrug classification datasets.** We perform binary classification on HIV (single-instance prediction) and SBAP (multi-instance prediction), and long-tailed classification on USPTO-50K (single-instance prediction) and DrugBank (multi-instance prediction). For each split and metric, the best method is **bolded** and the second best is underlined.

Dataset		HIV						SBAP						
Metric		AUPRC	Kappa	MCC	Weighted-F1	Micro-F1	Macro-F1	AUPRC	Kappa	MCC	Weighted-F1	Micro-F1	Macro-F1	
Random	Vanilla GCN	69.92	44.15	44.48	96.39	96.56	72.06	<u>78.17</u>	53.95	53.97	97.61	97.59	76.98	
	Class-rebalancing	BS	69.50	22.12	27.72	90.99	87.80	59.87	77.86	28.90	39.00	92.82	89.80	63.24
		CB_F	69.24	38.78	39.68	95.40	94.97	69.31	76.82	50.11	51.99	96.99	96.57	74.99
		CS	68.78	24.70	30.00	91.74	88.99	61.40	75.87	35.89	44.46	94.45	92.43	67.26
	Information augmentation	Mixup	71.25	45.72	45.85	<u>96.36</u>	<u>96.41</u>	72.85	78.23	55.48	55.52	<u>97.69</u>	<u>97.68</u>	<u>77.74</u>
		Remix	<u>70.96</u>	44.59	<u>45.09</u>	96.09	96.09	72.30	77.71	<u>54.54</u>	<u>54.52</u>	98.26	98.26	78.48
		DiVE	67.59	22.10	29.80	90.99	86.17	59.83	63.33	29.09	29.30	90.09	85.18	58.89
	Module Improvement	CDT	70.49	<u>44.65</u>	44.71	96.27	96.29	<u>72.33</u>	77.64	54.28	54.31	97.62	97.59	77.14
		Decoupling	69.60	37.96	38.50	95.43	95.06	68.95	76.75	52.31	53.91	97.17	96.82	76.10
		IB	66.52	19.39	26.28	89.44	85.25	57.92	62.32	28.58	29.67	89.06	83.68	56.60
		BBN	68.00	21.98	28.53	89.97	86.11	59.33	75.79	34.90	43.75	94.22	92.06	66.69
	Standard	Vanilla GCN	79.30	42.49	50.17	68.99	71.24	68.99	94.49	54.58	60.15	76.21	77.29	76.21
Class-rebalancing		BS	78.20	50.09	51.60	74.68	75.04	74.68	<u>95.25</u>	76.82	77.27	88.38	88.41	88.38
		CB_F	79.37	43.14	50.05	69.57	71.57	69.57	94.79	68.17	70.90	83.78	84.08	83.78
		CS	79.12	53.89	56.56	76.39	76.95	76.39	95.46	79.57	79.63	89.78	89.79	89.78
Information augmentation		Mixup	<u>79.65</u>	42.96	50.71	69.31	71.48	69.31	93.67	55.08	60.69	76.48	77.54	76.48
		Remix	79.28	42.05	50.77	69.99	71.84	68.23	93.38	55.96	62.39	77.98	79.09	78.95
		DiVE	79.73	<u>51.08</u>	52.25	<u>76.16</u>	<u>76.63</u>	75.01	91.28	70.63	71.26	86.00	86.23	86.01
Module Improvement		CDT	79.12	42.48	50.52	68.94	71.24	68.94	93.69	58.38	63.21	78.40	79.19	78.40
		Decoupling	78.50	46.28	52.66	71.52	73.14	71.52	93.83	62.96	66.45	80.98	81.48	80.98
		IB	78.71	50.68	51.50	75.14	75.34	75.14	90.82	69.73	69.75	84.87	84.87	84.87
		BBN	80.66	46.99	47.40	73.39	73.50	73.39	94.82	<u>78.22</u>	<u>78.52</u>	<u>89.09</u>	<u>89.11</u>	<u>89.09</u>
Dataset		USPTO-50K						DrugBank						
Metric		AUPRC	Kappa	MCC	Weighted-F1	Micro-F1	Macro-F1	AUPRC	Kappa	MCC	Weighted-F1	Micro-F1	Macro-F1	
Random	Vanilla GCN	96.55	95.00	95.01	95.99	96.00	92.70	93.91	93.04	93.04	94.12	94.13	88.47	
	Class-rebalancing	BS	96.61	94.75	94.75	95.83	95.79	92.24	94.85	91.10	91.14	92.86	92.42	72.22
		CB_F	95.23	94.28	94.29	95.47	95.42	92.26	70.95	82.18	82.22	85.13	84.92	80.63
		CS	96.42	93.73	93.74	95.01	94.97	92.25	89.24	72.10	72.57	75.83	75.57	71.19
	Information augmentation	Mixup	97.27	96.34	96.34	97.09	97.07	94.44	96.24	95.37	95.37	96.09	96.10	92.87
		Remix	<u>97.22</u>	96.47	96.48	97.21	97.18	94.55	97.33	95.70	95.71	96.37	96.38	95.17
		DiVE	96.21	94.68	94.68	95.79	95.70	92.79	90.36	80.22	80.30	83.45	83.29	79.40
	Module Improvement	CDT	96.78	94.95	94.95	95.98	95.95	92.70	82.48	70.54	71.63	78.77	73.50	51.45
		Decoupling	95.34	93.14	93.14	94.50	94.50	90.98	93.44	90.81	90.81	92.25	92.24	88.40
		IB	94.38	92.44	92.47	92.45	92.25	87.56	82.68	73.86	74.33	79.04	77.06	55.53
		BBN	96.72	94.11	94.13	95.40	95.26	92.14	92.24	90.32	90.33	92.38	91.81	83.07
	Standard	Vanilla GCN	97.31	91.28	91.35	92.15	92.15	92.15	95.15	89.25	89.41	86.96	89.38	86.96
Class-rebalancing		BS	97.77	92.91	92.93	93.59	93.62	93.59	96.47	<u>94.63</u>	<u>94.69</u>	93.11	<u>94.69</u>	92.58
		CB_F	96.78	93.41	93.44	94.11	94.07	94.11	80.75	90.44	90.59	88.60	90.55	88.09
		CS	97.79	91.93	91.97	92.76	92.73	92.76	95.74	<u>94.63</u>	<u>94.69</u>	<u>93.42</u>	<u>94.69</u>	<u>92.89</u>
Information augmentation		Mixup	<u>98.55</u>	94.68	94.72	95.19	95.21	95.19	97.15	85.71	86.15	83.48	85.88	83.48
		Remix	98.45	<u>94.74</u>	<u>94.77</u>	<u>95.25</u>	<u>95.27</u>	<u>95.25</u>	96.38	89.81	90.00	87.46	89.93	87.46
		DiVE	97.56	93.36	93.40	94.00	93.97	94.00	93.72	89.83	90.00	87.97	89.95	87.46
Module Improvement		CDT	97.88	93.10	93.13	93.78	93.79	93.78	93.96	91.04	91.12	88.78	91.15	88.29
		Decoupling	95.45	87.67	87.81	87.11	87.20	87.11	94.72	89.85	90.00	87.78	89.97	87.30
		IB	91.74	86.86	86.94	88.08	88.17	88.08	95.13	89.86	89.96	87.61	89.98	87.14
		BBN	98.76	95.82	95.82	96.25	96.23	96.25	95.69	95.23	95.30	94.14	95.28	93.61

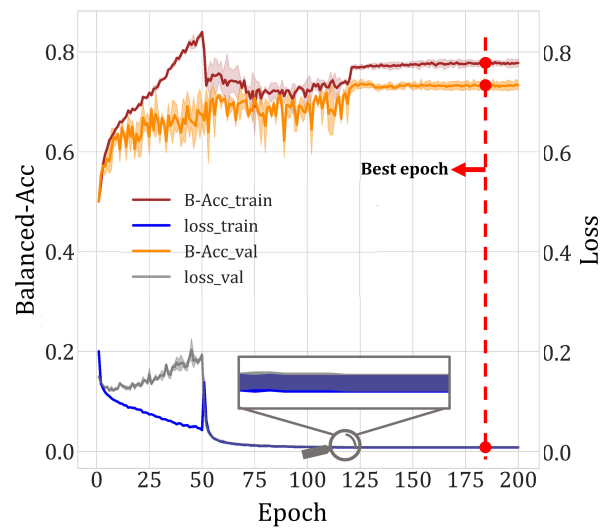


Figure 7: The training/validation curves on HIV dataset with GCN as backbone and **IB** as baseline. The curves are depicted on three runs.